



Upscaling of mass and heat transport applied to reactive packing catalytic porous media



O.A. Luévano-Rivas^a, J.J. Quiroz-Ramirez^{b,*}, V.A. Suarez-Toriello^b, B. Huerta-Rosas^c, E. Sánchez-Ramirez^c, J.G. Segovia-Hernández^c

^a CIATEC, A.C., Centro de Innovación Aplicada en Tecnologías Competitivas, Omega. 201, Industrial Delta, 37545 León, GTO, Mexico

^b CONACYT-CIATEC, A.C., Centro de Innovación Aplicada en Tecnologías Competitivas, Omega. 201, Industrial Delta, 37545 León, GTO, Mexico

^c Departamento de Ingeniería Química, Universidad de Guanajuato, Noria Alta s/n, Guanajuato, Gto. 36050, Mexico

HIGHLIGHTS

- The volume averaging method is used to upscaling the reactive catalytic packing.
- The computed effective coefficients include the effect of the structure of the catalytic pellets.
- The upscaled model is validated with comparisons with pore-scale simulations of the catalyst layer.
- The upscaled model as inputs in reactive multi-scale processes is plausible.

ARTICLE INFO

Article history:

Received 6 June 2022

Received in revised form 7 October 2022

Accepted 8 October 2022

Available online 23 October 2022

Keywords:

Reactive catalytic packing

Volume Averaging Theory

Heterogeneous reaction

Direct pore simulation

ABSTRACT

In various intensified processes, the presence of reactive catalytic packing is essential. These can be visualized as multiscale systems where a diverse mass, energy transfer, and chemical reaction occurs in the catalytic porous medium (i.e., the catalyst layer). This reactive microscopic scale structure influences efficiency. Given the hierarchical nature of the packing in the intensification systems, this paper proposes the derivation of an upscaled model that describes the first-order surface chemical reaction process in this catalyst layer. The upscaling is carried out using the volume averaging theory. The resulting model includes effective coefficients which depend on the transport and reaction parameters influenced by the unit cell geometry. The model is validated by comparing average temperature and concentration profiles obtained from numerical experiments using pore representations of a catalyst packing. The results show the effective parameters that can be used to design catalytic structures in the intensified process.

© 2022 Elsevier Ltd. All rights reserved.

1. Introduction

There are several processes of intensification that integrate heterogeneous catalytic reaction and separation process in a single multifunctional unit (e.g. catalytic distillation, reactive absorption, among others)(Stankiewicz, 2003). The advantages of this type of unit are related to high reaction conversion, low energy consumption, energy savings, and simple operation, and they have been successfully applied in multiple processes in the chemical engineering industry (Harmsen, 2007; Segovia-Hernández et al., 2015; Haase et al., 2022). The modeling of this system is complex because it integrates thermodynamics, hydrodynamics, mass and heat transfer, and chemical kinetics reaction, including the type,

geometry, and structure of internals and the influence characteristics of the catalytic packing, which affects the whole performance process significantly.

Using computational fluid dynamics (i.e., CFD) simulations is a tool that has been used extensively to characterize the hydrodynamics and mass transfer within the packed structure. Recently, the combination of CFD simulation processes has been proposed to relate the influence of catalytic packing structure on variables such as conversion, yield, and purity in catalytic distillation (Macfarlan et al., 2022). In these works, the results of CFD's hydrodynamic properties and mass transfer efficiency serve as input data for rigorous simulation processes. This tool has determined the hydrodynamic efficiency in the intensification process of catalytic separation columns using representative packing elements (van Baten and Krishna, 2002; Egorov et al., 2005). Thus, concerning the development of catalytic packing structures, the use of CFD

* Corresponding author.

E-mail address: jquiroz@ciatec.mx (J.J. Quiroz-Ramirez).

Nomenclature

a_v	interfacial surface area per unit cell volume (m^{-1})	$\langle p_\beta \rangle^\beta$	intrinsic averaged pressure in the β -phase, Pa
a_{v_h}	heat transfer coefficient per volume ($\text{W}/(\text{m}^3 \text{K})$)	\tilde{p}_β	pressure deviations in the β -phase, Pa
A_0	pre-exponential factor (m s^{-1})	Pe_ϕ	cell Péclet number on basis of mass diffusivity
\mathbf{b}_{mp}	closure variable for the m -phase associated to the source $\nabla \langle T_p \rangle^p$	Pe_T	cell Péclet number on basis of thermal diffusivity
$c_{A\beta}$	concentration of chemical species A in the fluid phase, (mol/m^3)	q	heat generation ($\text{kJ}/(\text{m}^3 \text{s})$)
$\langle c_{A\beta} \rangle^\beta$	intrinsic average concentration of chemical species A , mol/m^3	r	special closure variable for the heterogeneous chemical reaction case
\tilde{c}_A	spatial deviations of the concentration of chemical species A , mol/m^3	r_0	radius of the averaging volume V , m
c_p	specific heat capacity at constant pressure ($\text{J}/(\text{kg K})$)	\mathbf{r}_m ,	vector locating the m -phase with respect to the centroid of the averaging volume ($m = \beta, \sigma$) (m)
d_p	equivalent particle diameter, (m)	s_m	closure variable in the macroscopic equation for the m -phase associated to the source ($\langle T_m \rangle^m - \langle T_p \rangle^p$)
\mathbf{D}_β^*	total dispersion tensor under heterogeneous reaction, (m^2/s)	t	time, s
\mathcal{D}_β	molecular diffusion coefficient, (m^2/s)	t^*	characteristic process time, s
E	activation energy, (J/mol)	T_m	point temperature of the m -phase, (K)
F	arbitrary function of Taylor series	\mathbf{u}_{mp}	convective-like term for the m -phase associated to $\langle T_p \rangle^p$ ($m, p = \beta, \sigma$), (m/s)
\mathbf{f}_α	closure variable associated with the macroscopic source $\nabla \langle c_{A\beta} \rangle^\beta$ in the problem of dispersion with heterogeneous reaction, (m)	\mathbf{v}_β	velocity field, (m/s)
g_β	closure variable associated with the macroscopic source $\langle c_{A\beta} \rangle^\beta$ in the problem of dispersion with heterogeneous reaction	$\tilde{\mathbf{v}}_\beta$	spatial deviations of the velocity field, (m/s)
\mathbf{g}	gravitational acceleration vector, ms^{-2}	$\langle \mathbf{v}_\alpha \rangle$	superficial velocity field, (m/s)
H	heterogeneous reaction heat (kJ/mol)	$\langle v_\alpha \rangle$	magnitude of the superficial velocity, (m/s)
\mathbf{H}_β	effective permeability tensor (m^2)	V	averaging volume, (m^3)
\mathbf{l}	unit tensor	\mathcal{V}	magnitude of the averaging domain, (m^3)
k	heterogeneous reaction rate coefficient, (m/s)	x, y	Cartesian coordinates (m)
$k_{\langle T_\alpha \rangle^\alpha}$	heterogeneous reaction rate coefficient in terms of intrinsic temperature $\langle T_\sigma \rangle^\sigma$, s^{-1}	\mathbf{y}_α	position vector that locates points in the α -phase relative to the centroid of V , m
k_{eff}^*	effective reaction rate coefficient under dispersive conditions, s^{-1}		
k_m	thermal conductivity of the m -phase ($m = \beta, \sigma$) ($\text{W}/(\text{m K})$)	<i>Greek letters</i>	
K_{mp}	effective thermal coefficient in the macroscopic equation for the m -phase associated to $\langle T_p \rangle^p$, an asterisk indicates dispersive effects ($\text{W}/(\text{m K})$)	ε_m	volume fraction of the m -phase ($m = \beta, \sigma$)
L	characteristic length associated with volume averaged quantities, m	κ	ratio of thermal conductivities
ℓ_c	length of the unit cell, m	μ	dynamic viscosity ($\text{kg m}^{-1} \text{s}^{-1}$)
ℓ_m	characteristic length for the m -phase, (m)	ρ_m	density of the m -phase ($m = \beta, \sigma$), (kg m^{-3})
$\mathbf{n}_{\beta\sigma}$	unit normal vector pointing from the β -phase towards the σ -phase	ξ	heat distribution coefficient
p_β	pressure in the β -phase, Pa	ϕ ,	microscale Thiele modulus with heterogeneous reaction
		<i>Sub and superscripts</i>	
		β	fluid phase
		σ	solid phase
		<i>Special Symbols</i>	
		ϕ	deviation from intrinsic average
		$\langle \phi \rangle$	superficial average
		$\langle \phi \rangle^m$	intrinsic average for the m -phase, ($m = \beta, \sigma$)

has been frequently used to study the characteristics of fluid flow and mass transfer in the packing structure, obtaining acceptable results compared to experimental data (Mazarei Sotoodeh et al., 2018; Wang et al., 2020; Xue et al., 2021).

It has been pointed out that CFD simulations on the catalytic packing related to simulation processes are not enough to perform optimizations of the catalytic structure. This is because the efficiency is not solely influenced by the hydrodynamics and mass transfer characteristics of the catalytic packing internals but also involves the multicomponent mass transfer and the heterogeneous reaction process in the catalytic porous medium (i.e., catalyst layer) (Wang et al., 2017; Hong et al., 2021). Although hydrodynamic and vapor–liquid mass transfer can be simulated in representative catalytic packing units, the efficiency of the intensification process with reactive columns is additionally influenced by simultaneous heterogeneous chemical reactions and

mass transport of the components in the catalytic porous medium in the catalyst layer. This complex structure that conforms to the column may be prohibitively to simulate employing CFD due to the need for enormous required computational resources, limiting the application of this type of computational tool in process simulation and optimization schemes (Amini et al., 2019).

Despite these remarkable advances in the use of CFD modeling, for intensification process with reactive porous media, some alternatives can be applied to model the microscopic process of mass transfer and reaction process in the catalyst layer at a somewhat reasonable computational cost; considering that the determination of structural parameters of the catalyst layer is a factor that influences the efficiency of the catalytic packing. The reactive columns in intensification process can be conceptualized as a hierarchical system at different scales, ranging from the catalyst layer (microscopic scale) through intermediate stages such as catalytic packing

(Darcy or macroscopic scale) to the column (mega-scale), as shown in Fig. 1. The internal structure of the catalytic packing contains the catalyst layers in transfer units that form the complete catalytic packing column in intensification process. In contrast, the catalyst layers consist of a catalytic porous medium formed by catalytic particle arrays. Mass and heat transport and the heterogeneous chemical reaction occur in the reactive zones. Generally, in the reactive separation intensification process a catalyst layers is localized with vapor–liquid channels, such that most of the liquid carrying the reactant chemical species flow-through catalyst layers saturating them. The reactant chemical species diffuse within the microstructure of the catalyst layers due to the concentration gradient and react on the surface of the catalytic pellets. The reactant chemical species diffuse within the microstructure of the catalyst layers due to the concentration gradient and react on the surface of the catalytic pellets.

Consequently, this dispersion-reaction process within the catalyst layers has significantly influenced the whole process. Under this perspective of a hierarchical system of catalytic packing, it is plausible to propose the development of models based on upscaling methodologies. The deductions of upscaled models can be carried out by several available techniques such as volume averaging (Whitaker, 1999), homogenization (Mauri, 1991), or the thermodynamically constrained averaging theory (Gray and Miller, 2014). The resulting upscaled models using these techniques are usually written in terms of effective coefficients that can be calculated by solving ancillary closure problems on periodic representations of the microstructure of the porous medium. These coefficients characterize the transport from the pore scale to the macroscopic counterparts.

For processes involving mass and heat transfer with chemical reaction in a catalytic porous medium, such as the dispersion-reactive process in catalyst beds, various upscaling analyses using volume averaging have been proposed. In the transport of mass with reaction, the initial analysis works focused on diffusive processes coupled with heterogeneous chemical reactions in porous media (Ryan, 1983; Shapiro and Brenner, 1986; Shapiro and Brenner, 1988; Whitaker, 1987), extending later to upscale considering dispersion with heterogeneous chemical reaction with first order chemical kinetics (Ryan, 1983; Shapiro and Brenner, 1986; Whitaker, 1987; Valdes-Parada and Alvarez-Ramirez, 2010). The

effective coefficients determined in these models are shown to be essentially dependent on the parameters characterizing the nature and magnitude of the surface chemical reaction rate and velocity, influenced in turn by the essential geometrical characteristics of the unit cell used for the determination of the coefficients (Valdés-Parada et al., 2011; Valdés-Parada et al., 2017). Recently, more complex reaction kinetics have been considered in the derivation of upscaled models using the volume averaging theory; these include reversible and nonlinear reactions (e.g., Michaelis-Menten kinetics.), where explored a linearization of the nonlinear kinetics to reduce the mathematical complexity of the associated closure problems to close the macroscopic model (Wood et al., 2007; Heße et al., 2009; Porta et al., 2012; Lugo-Méndez et al., 2015; de los Santos-Sánchez et al., 2016; Qiu et al., 2017). One aspect of these studies is that they were performed under isothermal conditions. However, heterogeneous reaction processes are generally coupled to heat transfer processes with chemical reaction sources. Considering energy transport in porous media, upscaling analyses based on the volume averaging theory have been proposed, resulting in models based on the assumptions of local thermal equilibrium and non-equilibrium (Cheremisinoff, 1989; Whitaker, 1991; Quintard and Whitaker, 1993). The upscaled model results in one or two equations to describe the dispersive heat transport in porous media consisting of a fluid and a solid. The effective coefficients associated with the heat transfer mechanism, including interfacial heat transfer, are reported to be dependent mainly on the thermal conductivities of the phases, the flow velocity, and the geometry of the unit cell (Quintard et al., 1997). The upscaling of heat transfer with a homogeneous or heterogeneous heat source has been modeled assuming a constant and uniform source (Whitaker, 1986; Quintard and Whitaker, 2000). The above is generally not applicable for the case of a chemical reaction source which is usually coupled to the mass equations through a nonlinear Arrhenius law type equation. Recent work has considered this nonlinear heat source problem by obtaining a non-equilibrium model with upscaled equations that include effective coefficients that consider the heat generation rate associated with the chemical reaction (Yang et al., 2015a; Yang et al., 2015b).

Returning to the case study of the reactive columns in the intensification process, in the catalyst layer, the heterogeneous chemical

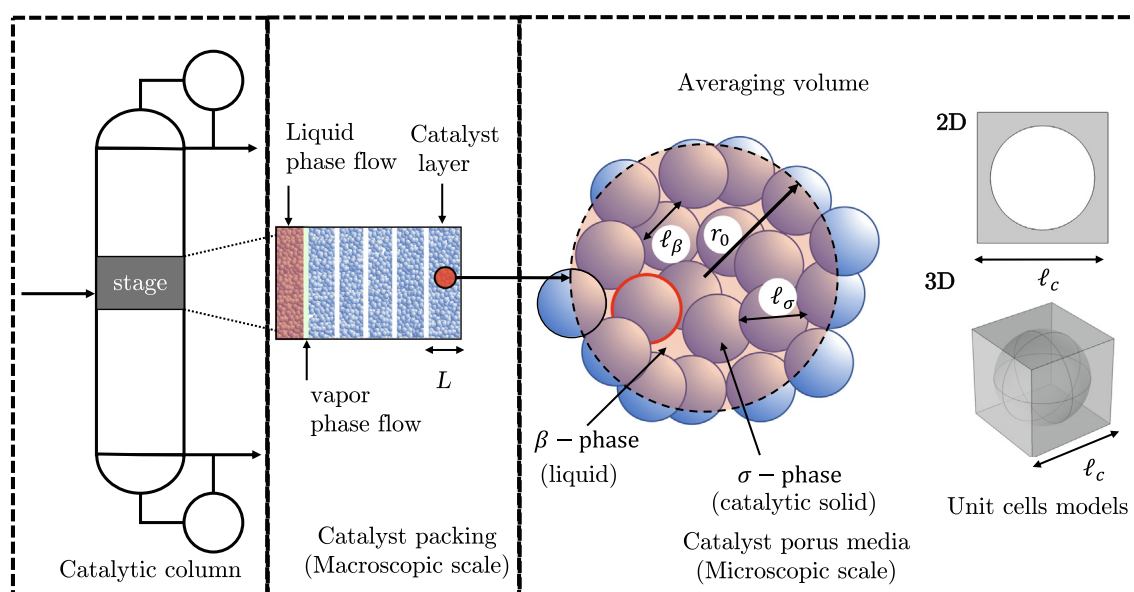


Fig. 1. Scales associated with general catalytic intensification column and averaging volume for solid catalytic particles and fluid liquid phase.

reaction occurs on the surface of the catalytic pellets; this process can be considered as a mass and heat transport coupled by a surface chemical reaction in a catalytic porous medium. Under the hierarchical scheme of the catalyst layer in a catalytic column, this paper proposes to deduce the valid upscaled model using the volume averaging theory for the dispersion/reaction process of the reactive zone formed by the catalyst layer. Since the structures of the catalyst layers influence the efficiency in the intensification process with catalytic packings, the resulting upscaled model and associated effective coefficients can be used to establish appropriate microstructures for the catalyst layers and eventually be used in the design and optimization studies global simulation process. For this purpose, in Section 2, the microscopic model that describes the reaction process in the catalyst layer is presented. We limit our analysis to considering a chemical species first-order Arrhenius-type heterogeneous reaction. The heat transport is in catalytic solid and fluid, including a heat source due to the surface reaction. In Section 3, we develop the macroscopic models for mass and heat transport with heterogeneous reactions using the upscaling approach given by the frame theory of the volume averaging theory. The upscaled closed models are presented in Section 4. Predictions of the effective coefficients of mass and heat in simple 2D and 3D representative structures of the catalyst layer also are presented in this section. The upscaled model is valid compared with pore-scale numerical simulation in 2D structures of the catalyst layer in Section 5. Finally, conclusions are drawn supporting the developed upscaled model, the predictions of the effective coefficients, and validated by numerical experiments in Section 6.

2. Pores-scale model

The hierarchical nature of the catalytic intensification process is represented in Fig. 1. We can consider that in the catalyst packing (Macroscopic scale), the flow liquid–vapor phase occurs only in the inter-region of the channels and catalyst layer, and the downward liquid flows to form a liquid film along the surface of catalyst layers. Therefore, the liquid phase saturates the catalytic porous media. The reactant chemical species are transported into the structure of catalyst layers under the concentration gradient and convection. The reactant species react on the catalyst pellet's surfaces and only occur below the bubble point temperature in the liquid phase. Thus, a multiphase liquid–vapor system is not considered within the catalytic porous medium. Analogously, the product species are transported onto the catalyst layer surface in the opposite direction, and mass transfer with the vapor phase occurs. In these processes, heat is produced due to the reaction on the catalyst pellet's surfaces.

The reaction process under consideration inside the catalyst layer, described before, can be established if we let us consider the catalyst pellets as a rigid and homogeneous medium that is fully saturated with a liquid phase (β -phase), as sketched in porous catalyst media of Fig. 1. We consider the process of diffusion and convection in the porous media involving a heterogeneous reaction at the surface of the solid phase (catalyst pellets), σ -phase, which is covered by the reactive material. The heat is transported by convection and conduction for the whole catalytic packing, which includes fluid and solid phases, with no contribution of convection for the last one. A source of heat is present due to the surface reaction. The radiation exchanges are not considered. The link between heat and mass transport gives by Arrhenius-type kinetic functions.

2.1. Microscopic model

Assuming that the fluid properties do not depend strongly on the temperature and concentrations, and the momentum balance

in the pores of the catalyst porous media can be considered independent of the mass and heat balances,

$$\nabla \cdot \mathbf{v}_\beta = 0, \text{ in the } \beta - \text{ phase} \quad (1a)$$

$$\rho_\beta \left(\frac{\partial \mathbf{v}_\beta}{\partial t} + \mathbf{v}_\beta \cdot \nabla \mathbf{v}_\beta \right) = -\nabla p_\beta + \rho_\beta \mathbf{g} + \mu_\beta \nabla^2 \mathbf{v}_\beta, \text{ in the } \beta - \text{ phase} \quad (1b)$$

$$\mathbf{v}_\beta = \mathbf{0}, \text{ at } \mathcal{A}_{\beta\sigma} \quad (1c)$$

In the above equations, ρ_β and μ_β represent the fluid density and viscosity. We assume the velocity of the liquid phase is such in the reactive zone that the liquid phase completely saturates the catalytic porous media. Considering the flow is steady and incompressible, the inertial term in Eq. (1b) can be considered negligible. The non-slip condition applies at $\mathcal{A}_{\beta\sigma}$. Recently, (Lasseux et al., 2016), the model for slightly compressible gas slip flow in porous media was developed by upscaling the pore-scale boundary value problem and a vapor phase model could be considered. Since accounting for the inertial effects provided a better representation for the computation of the velocity field, it increases the computational time. We suppose the catalytic reaction only occurs in the liquid phase saturating the catalytic packaging and no phase change occurs inside the catalytic layer.

Let us consider the transport process of diffusion and convection in a porous media for chemical species A carried by the fluid phase, involving a chemical reaction at the solid–fluid interface. For diluted species, the value of the diffusion coefficient is specified constant. For multicomponent non-dilute solutions, the process is more complex due to the diffusion coefficient corresponding to a diffusivity matrix (Vynnycky and Birgersson, 2003; Quintard et al., 2006). The chemical reaction could be a complex process that involves a series of reaction mechanisms; in this system, we simplified by assuming that the reaction of the A component reacts with in excess B component located at the interface of the solid and the fluid; assuming the reaction takes place until the component B is not exhausted. Additionally, the reaction products are assumed initially as passive components, and the transport description does not necessarily include them in the pore scale. The generalized reaction scheme for an exothermic reaction can be simplified as



The kinetic law of reaction is supposed to be a first-order law concerning chemical species A , and the Arrhenius equation represents the heterogeneous reaction rate,

$$s_{rxn} = kc_{A_\beta}; \quad k = A_0 e^{-E/RT_\sigma} \quad (3)$$

A_0 represents the pre-exponential factor, E is the activation energy, and R is the gas ideal constant. The first-order Arrhenius-type is used here to describe heterogeneous chemical reactions. The first-order Arrhenius-type describes the heterogeneous chemical reactions to simplify the analysis of the upscaling up process to be carried out in the following sections. However, it should be emphasized that different kinetics correspond to specific reaction mechanisms, and non-linear kinetics may be required. In the Eq. (3), We notice the reaction depends on both the concentration of chemical species A and T_σ is the temperature at the solid–fluid interface. Therefore thermal is coupled with mass transport. The reactive process described is represented through the following governing equations and boundary conditions for the transport of mass and heat at the pore-scale (*i.e.* the microscale)

$$\frac{\partial c_{A_\beta}}{\partial t} + \nabla \cdot (\mathbf{v} c_{A_\beta}) = \nabla \cdot (\mathcal{D}_\beta \nabla c_{A_\beta}), \text{ in } \beta - \text{ phase} \quad (4a)$$

$$-\mathbf{n}_{\beta\sigma} \cdot \mathcal{D}_\beta \nabla c_{A_\beta} = s_{rxn}, \text{ in } \mathcal{A}_{\beta\sigma} \quad (4b)$$

where \mathcal{D}_β is the molecular diffusion coefficient that, as mentioned before, is a constant value. The microscale formulation is completed with the corresponding boundary conditions at macroscale boundaries. The corresponding energy balance for the described reactive system is

$$(\rho c_p)_\beta \left[\frac{\partial T_\beta}{\partial t} + \nabla \cdot (\mathbf{v} T_\beta) \right] = \nabla \cdot (k_\beta \nabla T_\beta), \text{ in } \beta - \text{ phase} \quad (5a)$$

$$(\rho c_p)_\sigma \frac{\partial T_\sigma}{\partial t} = \nabla \cdot (k_\sigma \nabla T_\sigma), \text{ in } \sigma - \text{ phase} \quad (5b)$$

$$\mathbf{n}_{\beta\sigma} \cdot k_\beta \nabla T_\beta = \mathbf{n}_{\beta\sigma} \cdot k_\sigma \nabla T_\sigma + s_{rxn} H, \text{ at } \mathcal{A}_{\beta\sigma} \quad (5c)$$

$$T_\beta = T_\sigma, \text{ at } \mathcal{A}_{\beta\sigma} \quad (5d)$$

where $\mathbf{n}_{\beta\sigma}$ is the unit normal vector pointing from β - to σ - phase ($\mathbf{n}_{\beta\sigma} = -\mathbf{n}_{\sigma\beta}$). The velocity field, \mathbf{v}_β , is obtained by solving the Stokes or Navier–Stokes equations under the assumptions of E*qs. (1a)–(1c). H represents the heat of the reaction, which is assumed constant and independent of temperature. Theoretically, H depends on the temperature and volume heat capacities of the fluid and solid phases, $(\rho c_p)_m$, and thermal conductivity, k_m , $m = \beta, \sigma$ respectively. However, as an initial approximation, it is satisfactory to consider constants for simulation purposes. For practical cases, the heat given off by the heterogeneous chemical reaction at the surface of the catalytic particles, H , can be considered negligible (Lei et al., 2009). However, in this work, it is included through the boundary condition in the microscopic model (Eq. 5c) to emphasize the contribution of the reactive heat source in the upscaling processes, which will perform in the following sections. Therefore, the energy chemical reaction contributions in the upscaled model and the subsequent global modeling could take into the duty energy requirements (Goortani et al., 2015). To conclude this section, some limitations of the proposed model should be pointed out, especially in the approach to future more complex modeling of intensified reaction separation systems. Firstly, it has been considered that the reactants and products are below the bubble point temperature. Therefore a vapor–liquid mixture, essential in describing this type of intensified system, is not considered. Furthermore, multicomponent transport is not included, and the consideration of irreversible reactions are strong assumption in this work. However, the scaling perspective that will be developed in the following section under the proposed assumptions and simplifications is a novel way to approach the systematic application of the upscaling method to address this type of complex system.

3. Upscaling procedure

The upscaling procedure of the boundary value problems, presented in the previous section, is applied to obtain the macroscopic closed model. Different methodologies could be used to derive the upscaled model, for instance, homogenization (Sanchez-Palencia, 1980), or volume averaging theory (Whitaker, 1999). In the present work, we use the latter omitting the details discussed extensively in the literature. Briefly, the averaging process is carried out by defining an Averaging volume, \mathcal{V} , of measure V , and characteristic size r_0 , that contains both catalytic solid and fluid phase, such as sketched in Fig. 1. The averaging volume contains all the necessary structural information (Representative Elementary Volume (REV) (Bear and Cheng, 2018)). The characteristic size of the averaging domain is usually constrained under the assumption of following length-scale separation (Wood and Valdés-Parada, 2013)

$$\ell_m, \ll r_0 \ll L, m = \beta, \sigma \quad (6)$$

here ℓ_m represents the characteristic length associated with the β - and σ -phase (e.g. the pore diameter), and L is the characteristic length associated with the macro-scale. Over the averaging volume,

the macroscale physical quantities in the reaction region, ψ_m , are defined by the superficial and intrinsic averaging operators,

$$\langle \psi_m \rangle = \frac{1}{V} \int_{\mathcal{V}_m} \psi_m dV, \quad m = \beta, \sigma, \quad (7a)$$

$$\langle \psi_m \rangle^m = \frac{1}{V_m} \int_{\mathcal{V}_m} \psi_m dV, \quad (7b)$$

here ψ_m represent both the concentration and temperature, c_A and T_m and \mathcal{V}_m (with volume V_m) represents the proportion of \mathcal{V} occupied by the fluid or the solid catalytic phase in the volume \mathcal{V} . These two averages are related by

$$\langle \psi_m \rangle = \frac{V_m}{V} \langle \psi_m \rangle^m \quad (8)$$

where the ratio $\varepsilon_m = V_m/V$ is the porosity, which is suppose constant. The averaging process implies the application of the intrinsic averaging operator to the microscale equations, followed by exchange differentiation and integration using the spatial averaging theorem (Howes and Whitaker, 1985; Gray and Miller, 2013). The resulting average equations contain both macroscale ($\langle \psi_m \rangle$) and microscale (ψ_m) quantities. It is necessary to express the pointwise quantities in terms of their averages and corresponding spatial deviations according to Gray's (Gray, 1975) spatial decomposition

$$\psi_m = \langle \psi_m \rangle^m + \hat{\psi}_m, \quad m = \beta, \sigma \quad (9)$$

The upscaling of the reaction process model in the reactive region of this simply intensified column begins by analyzing the flow in the porous catalyst layer. The liquid phase flow in porous medium has been studied extensively, and details are available elsewhere (Whitaker, 1996; Whitaker, 1999). For momentum transport of the β -phase, described in the Eq. (1a)), the resulting equations from the upscaling process is the Darcy–Forchheimer equation which can be resembles to a Darcy's law as

$$\langle \mathbf{v}_\beta \rangle = - \frac{\mathbf{H}_\beta}{\mu_\beta} \cdot \left(\nabla \langle p_\beta \rangle^\beta - \rho_\beta \mathbf{g} \right) \quad (10)$$

where the tensor \mathbf{H}_β is the apparent permeability defined as $\mathbf{H}_\beta^{-1} = \mathbf{K}_\beta^{-1} \cdot (\mathbf{I} + \mathbf{F}_\beta)$ where \mathbf{K}_β and \mathbf{F}_β are the intrinsic permeability tensor and the Forchheimer correction tensor, respectively; considering no inertial, the tensor \mathbf{H}_β resembles to the intrinsic permeability \mathbf{K}_β . The computation of the permeability coefficient is an achievement in solving the associated closure problem in the periodic representation of the porous catalyst layer, where the reaction occurs. In general, in this work, we use the simple geometries involving circle (2D) and sphere (3D) obstacles in unit cells to represent the catalytic particles in the porous catalyst layer, as shown in Fig. 1. With the aim to center the discussion in this work on the mass and heat transfer upscaling for the reaction process in the catalyst layer, the details in the solution of the predictions of permeability coefficient are summarized in the A. The upscaling model for a single-fluid in the porous catalyst layer is closed using the results of the longitudinal intrinsic permeability ($K_{\beta,xx}$), which results can fit ($R^2 = 0.999$) as functionality with the porosity for 2D and 3D unit cells, as follows

$$\frac{K_{\beta,xx}}{\ell_c^2} = -8.293 \times 10^{-4} + 1.048 \times 10^{-4} e^{6.575\varepsilon_\beta} \varepsilon_\beta \in (0.30.8) \quad 2D \quad (11a)$$

$$\frac{K_{\beta,xx}}{\ell_c^2} = -1.135 \times 10^{-3} + 1.841 \times 10^{-4} e^{6.039\varepsilon_\beta} \varepsilon_\beta \in (0.50.8) \quad 3D \quad (11b)$$

The unit cells can involve various arrangements or geometries with the predictive perspective of the influence on the velocity rate in the reactive system present in intensified systems (Wang et al., 2017; Wang et al., 2020). Here we selected the most straightforward geometry to represent the structure of a catalytic particle in the

catalyst layer. However, the geometry of the unit cell is not constrained to these 2D and 3D geometries; complex models or diverse geometries can use to compute the effective coefficients included in the Eq. 10.

The deduction of the upscaling mass and heat transport model with the surface reaction is presented in more detail in the following paragraphs using the VAM. This model will describe the reactive process reactive region (i.e., catalytic porous media). The upscaling continues with the mass transport of the component A in the reactive process in the catalyst layer. The systematical applications of the volume averaging operators over the pore-scale model, given by the E*q. (4), results in the following macroscopic mass transport model for the chemical component A,

$$\begin{aligned} & \varepsilon_\beta \frac{\partial \langle c_{A\beta} \rangle^\beta}{\partial t} + \nabla \cdot \left(\varepsilon_\beta \langle c_{A\beta} \rangle^\beta \langle \mathbf{v}_\beta \rangle^\beta \right) \\ & = \nabla \cdot \left[\varepsilon_\beta \mathcal{D}_\beta \left(\nabla \langle c_{A\beta} \rangle^\beta + \frac{1}{V_\beta} \int_{\mathcal{A}_{\beta\sigma}} \mathbf{n}_{\beta\sigma} \tilde{c}_{A\beta} dA \right) - \varepsilon_\beta \langle \tilde{c}_{A\beta} \tilde{\mathbf{v}}_\beta \rangle^\beta \right] \\ & \quad - \frac{1}{V} \int_{\mathcal{A}_{\beta\sigma}} s_{rxn} dA \end{aligned} \quad (12)$$

The last term includes the heterogeneous reaction contribution in the macroscopic mass equation. In the other hand, the result of averaging the governing equations microscopic equation, E*q. 5 (a) and (b), the heat transfer in both phases, the transport fluid and catalytic solid particle with surface reaction, result as

$$\begin{aligned} & \varepsilon_\beta (\rho c_p)_\beta \frac{\langle T_\beta \rangle^\beta}{\partial t} + \varepsilon_\beta (\rho c_p)_\beta \langle \mathbf{v}_\beta \rangle^\beta \cdot \nabla \langle T_\beta \rangle^\beta \\ & = \nabla \cdot \left[\varepsilon_\beta k_\beta \left(\nabla \langle T_\beta \rangle^\beta + \frac{1}{V_\beta} \int_{\mathcal{A}_{\beta\sigma}} \mathbf{n}_{\beta\sigma} \tilde{T}_\beta dA \right) \right] - (\rho c_p)_\beta \nabla \\ & \quad \cdot \langle \tilde{T}_\beta \tilde{\mathbf{v}}_\beta \rangle + \frac{1}{V} \int_{\mathcal{A}_{\beta\sigma}} \mathbf{n}_{\beta\sigma} \cdot k_\beta \nabla T_\beta dA \end{aligned} \quad (13)$$

$$\begin{aligned} \varepsilon_\sigma (\rho c_p)_\sigma \frac{\langle T_\sigma \rangle^\sigma}{\partial t} & = \nabla \cdot \left[\varepsilon_\beta k_\sigma \left(\nabla \langle T_\sigma \rangle^\sigma + \frac{1}{V_\sigma} \int_{\mathcal{A}_{\sigma\beta}} \mathbf{n}_{\sigma\beta} \tilde{T}_\sigma dA \right) \right] \\ & \quad + \frac{1}{V} \int_{\mathcal{A}_{\sigma\beta}} \mathbf{n}_{\sigma\beta} \cdot k_\beta \nabla T_\sigma dA \end{aligned} \quad (14)$$

In these macroscopic heat transport equations, the first and second integral terms on the right of Eq. (13) and (14) will be related to the hydrodynamic dispersive-diffusive heat transport. The third integral term, written in pore-scale temperature in both equations, includes implicit the source given by heterogeneous reaction in the surface $\mathcal{A}_{\beta\sigma}$, as is indicated by boundary condition Eq. (5c). Additional details in the development of the averaging equation can be found in (Whitaker, 1999). The main characteristics in the Eqs. (12)–(14) are they contains both, macroscopic, $\langle \psi_m \rangle^m$, and deviation quantities, $\tilde{\psi}_m$. Under the VAM framework, determining the functionality of the quantity deviations with the corresponding average quantities is known as *closure*. This procedure involves, in general, the following algorithm: (1) derivative of the balance equations for $\tilde{\psi}_m$ and boundary conditions based on the expression in the Eq. (9); (2) impose a set of reasonable assumptions [expressed in terms of upscaling laws (Whitaker, 1999; Wood, 2009; Wood and Valdés-Parada, 2013)] to simplify the deviations governing equations and (3) finally derive a formal solution of the boundary-value problem for deviations. For the mass transfer, the concentration deviation equation is achieved by subtracting the Eq. (12) to their respective microscopic counterpart in the Eq. (4a), which result in the following governing equations for deviations of component A in the fluid.

$$\begin{aligned} & \frac{\partial \tilde{c}_{A\beta}}{\partial t} + \nabla \cdot \left(\tilde{\mathbf{v}}_\beta \langle c_{A\beta} \rangle^\beta \right) + \nabla \cdot \left(\mathbf{v}_\beta \tilde{c}_{A\beta} \right) \\ & = \nabla \cdot \left(\mathcal{D}_\beta \nabla \tilde{c}_{A\beta} \right) - \nabla \cdot \left[\frac{\mathcal{D}_\beta}{V_\beta} \int_{\mathcal{A}_{\beta\sigma}} \mathbf{n}_{\beta\sigma} \tilde{c}_{A\beta} dA - \langle \tilde{c}_{A\beta} \tilde{\mathbf{v}}_\beta \rangle^\beta \right] - \frac{1}{V_\beta} \\ & \quad \times \int_{\mathcal{A}_{\beta\sigma}} s_{rxn} dA \end{aligned} \quad (15)$$

We can simplify this expression based on the order of magnitude estimates for the accumulation and diffusive terms based on the separation of length scales, $\ell_\beta \ll L$. Besides, the closure problem for mass can be treated as a quasi-stable under assumption of characteristic time constraints, ($\ell_\beta^2 / \mathcal{D}_\beta \ll t^*$) (Whitaker, 1999; Valdés-Parada et al., 2011; Valdés-Parada et al., 2017). As a result, it is satisfied that

$$\begin{aligned} \frac{\partial \tilde{c}_{A\beta}}{\partial t} & \ll \mathcal{D}_\beta \nabla^2 \tilde{c}_{A\beta}, \quad \nabla \cdot \left[\frac{\mathcal{D}_\beta}{V_\beta} \int_{\mathcal{A}_{\beta\sigma}} \mathbf{n}_{\beta\sigma} \tilde{c}_{A\beta} dA \right] \\ & \ll \mathcal{D}_\beta \nabla^2 \tilde{c}_{A\beta}, \quad \varepsilon_\beta^{-1} \nabla \cdot \left(\tilde{\mathbf{v}}_\beta \tilde{c}_{A\beta} \right) \ll \tilde{\mathbf{v}}_\beta \cdot \nabla \tilde{c}_{A\beta} \end{aligned} \quad (16)$$

and the Eq. (15) simplifies to

$$\tilde{\mathbf{v}}_\beta \cdot \nabla \langle c_{A\beta} \rangle^\beta + \mathbf{v}_\beta \cdot \nabla \tilde{c}_{A\beta} = \nabla \cdot \left(\nabla \mathcal{D}_\beta \tilde{c}_{A\beta} \right) + \frac{1}{V_\beta} \int_{\mathcal{A}_{\beta\sigma}} s_{rxn} dA \quad (17)$$

Performing a similar analysis, we obtain the governing equations for fluid and solid catalytic temperature deviations by subtracting the Eqs. (13) and (14) to Eqs (5a) and (5b), respectively, leading to

$$\begin{aligned} & (\rho c_p)_\beta \left(\frac{\tilde{T}_\beta}{\partial t} + \mathbf{v}_\beta \cdot \nabla \tilde{T}_\beta + \tilde{\mathbf{v}}_\beta \cdot \nabla \langle T_\beta \rangle^\beta \right) \\ & = \nabla \cdot \left(k_\beta \nabla \tilde{T}_\beta \right) - \varepsilon_\beta^{-1} \nabla \cdot \left[\frac{k_\beta}{\mathcal{V}'} \int_{\mathcal{A}_{\beta\sigma}} \mathbf{n}_{\beta\sigma} \tilde{T}_\beta dA \right] + \varepsilon_\beta^{-1} (\rho c_p)_\beta \nabla \\ & \quad \cdot \langle \tilde{\mathbf{v}}_\beta \tilde{T}_\beta \rangle - \frac{\varepsilon_\beta^{-1}}{\mathcal{V}'} \int_{\mathcal{A}_{\beta\sigma}} \mathbf{n}_{\beta\sigma} \cdot k_\beta \nabla \tilde{T}_\beta dA, \text{ in } \beta - \text{phase} \end{aligned} \quad (18)$$

$$\begin{aligned} (\rho c_p)_\sigma \frac{\tilde{T}_\sigma}{\partial t} & = \nabla \cdot \left(k_\sigma \nabla \tilde{T}_\sigma \right) - \varepsilon_\sigma^{-1} \nabla \cdot \left[\frac{k_\sigma}{\mathcal{V}'} \int_{\mathcal{A}_{\sigma\beta}} \mathbf{n}_{\sigma\beta} \tilde{T}_\sigma dA \right] - \frac{\varepsilon_\sigma^{-1}}{\mathcal{V}'} \\ & \quad \times \int_{\mathcal{A}_{\sigma\beta}} \mathbf{n}_{\sigma\beta} \cdot k_\sigma \nabla \tilde{T}_\sigma dA, \text{ in } \sigma - \text{phase} \end{aligned} \quad (19)$$

Under similar assumption used in the mass analysis, the separation of length-scale, $\ell_\beta, \ell_\gamma \ll L$, and time-scale constraints for fluid phase, $\ell_\beta^2 / \alpha_\beta / (\frac{v_\beta \ell_\beta}{\alpha_\beta} + 1) \ll t^*$, and catalytic solid, $\frac{\ell_\sigma^2}{\alpha_\sigma} \ll t^*$, where the thermal diffusivities are $\alpha_\beta = k_\beta / (\rho c_p)_\beta$ and $\alpha_\sigma = k_\sigma / (\rho c_p)_\sigma$, the following inequalities are satisfied

$$\begin{aligned} \varepsilon_\beta^{-1} \nabla \cdot \left[\frac{k_\beta}{\mathcal{V}'} \int_{\mathcal{A}_{\beta\sigma}} \mathbf{n}_{\beta\sigma} \tilde{T}_\beta dA \right] & \ll \nabla \cdot \left(k_\beta \nabla \tilde{T}_\beta \right), \quad \varepsilon_\sigma^{-1} \nabla \\ & \quad \cdot \left[\frac{k_\sigma}{\mathcal{V}'} \int_{\mathcal{A}_{\sigma\beta}} \mathbf{n}_{\sigma\beta} \tilde{T}_\sigma dA \right] \ll \nabla \cdot \left(k_\sigma \nabla \tilde{T}_\sigma \right) \end{aligned} \quad (20a)$$

$$\begin{aligned} \varepsilon_\beta^{-1} \nabla \cdot \langle \tilde{T}_\beta \tilde{\mathbf{v}}_\beta \rangle^\beta & \ll \mathbf{v}_\beta \cdot \nabla \tilde{T}_\beta, \quad \frac{\partial \tilde{T}_\beta}{\partial t} \\ & \ll -(\rho c_p)_\beta \mathbf{v}_\beta \cdot \nabla \tilde{T}_\beta + (\rho c_p)_\beta^{-1} \nabla \\ & \quad \cdot \left(k_\beta \nabla \tilde{T}_\beta \right), \quad \frac{\partial \tilde{T}_\sigma}{\partial t} \ll (\rho c_p)_\sigma^{-1} \nabla \cdot \left(k_\sigma \nabla \tilde{T}_\sigma \right) \end{aligned} \quad (20b)$$

and the governing equations for fluid and solid temperature deviations, Eqs. 18,19 are written as

$$\begin{aligned}
& (\rho c_p)_\beta (\mathbf{v}_\beta \cdot \nabla \tilde{T}_\beta + \tilde{\mathbf{v}}_\beta \cdot \nabla \langle T_\beta \rangle^\beta) \\
& = \nabla \cdot (k_\beta \nabla \tilde{T}_\beta) - \frac{\varepsilon_\beta^{-1} k_\beta}{\mathcal{V}} \int_{\mathcal{A}_{\beta\sigma}} \mathbf{n}_{\beta\sigma} \cdot \nabla \tilde{T}_\beta dA, \text{ in } \beta \text{ - phase} \quad (21)
\end{aligned}$$

$$0 = \nabla \cdot (k_\sigma \nabla \tilde{T}_\sigma) - \frac{\varepsilon_\sigma^{-1} k_\sigma}{\mathcal{V}} \int_{A_{\sigma\beta}} \mathbf{n}_{\sigma\beta} \cdot \nabla \tilde{T}_\sigma dA, \text{ in } \sigma \text{ - phase} \quad (22)$$

The corresponding boundary conditions at the interface of concentration and temperature deviations are obtained by applying the spatial decomposition, Eq. (9), in Eqs. (4b), (5c) and (5d). The results are expressed as follows

$$-\mathbf{n}_{\beta\sigma} \cdot \mathcal{D}_\beta \nabla \tilde{c}_{A\beta} = -\mathbf{n}_{\beta\sigma} \cdot \mathcal{D}_\beta \nabla \langle c_{A\beta} \rangle^\beta + s_{rxn} \mathbf{a} \cdot \mathcal{A}_{\beta\sigma} \quad (23a)$$

$$\tilde{T}_\beta = \tilde{T}_\sigma - (\langle T_\beta \rangle^\beta - \langle T_\sigma \rangle^\sigma), \mathbf{a} \cdot \mathcal{A}_{\beta\sigma} \quad (23b)$$

$$\begin{aligned}
-\mathbf{n}_{\beta\sigma} \cdot k_\beta \nabla \tilde{T}_\beta &= -\mathbf{n}_{\beta\sigma} \cdot k_\sigma \nabla \tilde{T}_\sigma - \mathbf{n}_{\beta\sigma} \cdot k_\sigma \nabla \langle T_\sigma \rangle^\sigma \\
&+ \mathbf{n}_{\beta\sigma} \cdot k_\beta \nabla \langle T_\beta \rangle^\beta + s_{rxn} H \quad (23c)
\end{aligned}$$

In addition, a convenient assumption is that the closure problem domain solution can be considered a periodic unit cell representing the essential pore-scale structure. In essence, this assumption constitutes an upscaling postulate (Wood and Valdés-Parada, 2013), and we can impose the periodic boundary conditions, which implies the average constraints for the deviations fields associated with the loss of the information of the macroscopic boundary conditions,

$$\tilde{\psi}_m(\mathbf{r}) = \tilde{\psi}_m(\mathbf{r} + \mathbf{l}_k), k = 1, 2, 3; \langle \tilde{\psi}_m \rangle^m = 0, \quad m = \beta, \sigma \quad (24)$$

where $\mathbf{l}_k, k = 1, 2, 3$, are the periodic lattice vectors of the unit cell. For the analysis of the non-isothermal catalytic region in the closure problem, the previous closure problems deduction is consistent with similar treatments for the mass and heat transport in porous media (Valdés-Parada and Alvarez-Ramirez, 2010; Aguilar-Madera et al., 2011; Valdés-Parada et al., 2020).

An aspect of the closure problems deduced above is the linkage they present through the surface chemical reaction. Because of these, we direct attention to the reaction rate s_{rxn} , which is explicit on the microscopic temperature and the concentration of chemical species A via the Eq. (3). Exploring how to express the first-order reaction rate equation as functionality in terms of deviations and average quantities of phase temperatures and concentration is necessary. Thus, it requires expressing the first-order reaction rate equation as functionality in terms of deviations and average quantities of phase temperatures and concentration. We are concerned with expressing the Eq. (3) in terms of only the concentration deviations $\tilde{c}_{A\beta}$ in order to avoid the non-linear coupling in the interfaces of temperature and concentration deviations in the solution of the closure problem. The above allows the inclusion of a non-constant surface reaction rate in the derivation of the scaling model, in contrast to previous models for mass transport, which consider the reaction rate as constant. (Valdés-Parada et al., 2020). To achieve the analysis of the reaction rate, we define as the first instance an arbitrary function F according to the multivariate Taylor series expansion (Yang et al., 2015a), as follows,

$$\begin{aligned}
F(T_m, c_{A\beta}) &= F(\langle T_m \rangle^m, \langle c_{A\beta} \rangle^\beta) + (T_m - \langle T_m \rangle^m) \\
&\frac{\partial F}{\partial T_m} \Big|_{T_m=\langle T_m \rangle^m, c_{A\beta}=\langle c_{A\beta} \rangle^\beta} + (c_{A\beta} - \langle c_{A\beta} \rangle^\beta) \frac{\partial F}{\partial c_{A\beta}} \Big|_{T_m=\langle T_m \rangle^m, c_{A\beta}=\langle c_{A\beta} \rangle^\beta} + \dots \quad (25)
\end{aligned}$$

Using the spatial decomposition, Eq. (9), and based on the assumption of periodicity (Lugo-Méndez et al., 2015), the Taylor series can be expressed as

$$\begin{aligned}
F(T_m, c_{A\beta}) &= F(\langle T_m \rangle^m, \langle c_{A\beta} \rangle^\beta) \\
&+ \tilde{T}_m \frac{\partial F}{\partial T_m} \Big|_{T_m=\langle T_m \rangle^m, c_{A\beta}=\langle c_{A\beta} \rangle^\beta} + \tilde{c}_{A\beta} \frac{\partial F}{\partial c_{A\beta}} \Big|_{T_m=\langle T_m \rangle^m, c_{A\beta}=\langle c_{A\beta} \rangle^\beta} + \dots \quad (26)
\end{aligned}$$

Applying a similar expansion of Eq. (26), is valid express the reaction rate, s_{rxn} , Eq. (3) in terms of deviations of temperature of the catalytic solid, \tilde{T}_σ and concentration of reactant A , $\tilde{c}_{A\beta}$ at the interface conditions, and the average temperature and concentration, $\langle T_\sigma \rangle^\sigma$ and $\langle c_{A\beta} \rangle^\beta$ as follows

$$\begin{aligned}
s_{rxn} &= A_0 e^{-E/R(T_\sigma)^\sigma} \langle c_{A\beta} \rangle^\beta + A_0 e^{-E/R(T_\sigma)^\sigma} \tilde{c}_{A\beta} \\
&+ \tilde{T}_\sigma \left(\frac{E}{R(T_\sigma)^\sigma} \right) A_0 e^{-E/R(T_\sigma)^\sigma} \langle c_{A\beta} \rangle^\beta + \dots \quad (27)
\end{aligned}$$

An analogous expansion in terms of \tilde{T}_β and $\langle T_\beta \rangle^\beta$, leads to

$$\begin{aligned}
s_{rxn} &= A_0 e^{-E/R(T_\beta)^\beta} \langle c_{A\beta} \rangle^\beta + A_0 e^{-E/R(T_\beta)^\beta} \tilde{c}_{A\beta} \\
&+ \tilde{T}_\beta \left(\frac{A_0 E}{R(T_\beta)^\beta} \right) e^{-E/R(T_\beta)^\beta} \langle c_{A\beta} \rangle^\beta + \dots \quad (28)
\end{aligned}$$

Equating the Eq. (27) and Eq. (28), and substituting the result in the boundary condition at $A_{\beta\sigma}$ of closure problem, Eq (23b), the expression for deviation \tilde{T}_σ is write as

$$\begin{aligned}
\tilde{T}_\sigma &= \frac{\frac{E}{R(T_\beta)^\beta} e^{-E/R(T_\beta)^\beta} (\langle T_\sigma \rangle^\sigma - \langle T_\beta \rangle^\beta) - (e^{-E/R(T_\sigma)^\sigma} - e^{-E/R(T_\beta)^\beta})}{\frac{E}{R(T_\sigma)^\sigma} e^{-E/R(T_\sigma)^\sigma} - \frac{E}{R(T_\beta)^\beta} e^{-E/R(T_\beta)^\beta}} \\
&- \frac{(e^{-E/R(T_\sigma)^\sigma} - e^{-E/R(T_\beta)^\beta})}{\frac{E}{R(T_\sigma)^\sigma} e^{-E/R(T_\sigma)^\sigma} - \frac{E}{R(T_\beta)^\beta} e^{-E/R(T_\beta)^\beta}} \frac{\tilde{c}_{A\beta}}{\langle c_{A\beta} \rangle^\beta} \quad (29)
\end{aligned}$$

A similar expression can be carried out for the deviations of the temperature \tilde{T}_β . However, the solid catalytic temperature is selected considering that the average temperature of the solid is intrinsically related to the surface reaction at $A_{\beta\sigma}$. The result of substituting the Eq. (29) into the Eq. (28) is the required expression for chemical reaction rate, which only depends on concentration $\tilde{c}_{A\beta}$ deviations and macroscopic average quantities, written as

$$s_{rxn} = k_{(T_\sigma)^\sigma} (\omega_1 \langle c_{A\beta} \rangle^\beta + \omega_2 \tilde{c}_{A\beta}) \quad (30)$$

where $k_{(T_\sigma)^\sigma}$ is the average Arrhenius reaction rate coefficient written in terms of the average temperature of the solid catalytic phase, as follows

$$k_{(T_\sigma)^\sigma} = A_0 e^{-E/R(T_\sigma)^\sigma} \quad (31)$$

$$\omega_1 = \left(\omega_2 + \frac{\frac{E}{R} \langle (T_\beta)^\beta \rangle^2 e^{-E/R(T_\beta)^\beta} (\langle T_\sigma \rangle^\sigma - \langle T_\beta \rangle^\beta)}{e^{-E/R(T_\sigma)^\sigma} - \left(\frac{\langle T_\sigma \rangle^\sigma}{\langle T_\beta \rangle^\beta} \right)^2 e^{-E/R(T_\beta)^\beta}} = C_1 (\langle T_\sigma \rangle^\sigma, \langle T_\beta \rangle^\beta) \right)$$

$$\omega_2 = \left(1 - \frac{e^{-E/R(T_\sigma)^\sigma} - e^{-E/R(T_\beta)^\beta}}{e^{-E/R(T_\sigma)^\sigma} - \left(\frac{\langle T_\sigma \rangle^\sigma}{\langle T_\beta \rangle^\beta} \right)^2 e^{-E/R(T_\beta)^\beta}} = C_2 (\langle T_\sigma \rangle^\sigma, \langle T_\beta \rangle^\beta) \right) \quad (32)$$

The subscript $\langle T_\sigma \rangle^\sigma$ indicates the average temperature of the catalytic solid is the reference temperature for the surface reaction in the upscaling models. An exhaustive analysis of these expressions is required to evaluate circumstances that the ratios present in ω_1 and ω_2 definitions can be discarded. This could be done, on basis of the use of macroscopic deviations, as is proposed in the analysis of *local thermal equilibrium* in the *passive* (non-reaction) heat transfer process in porous media (Whitaker, 1986; Quintard et al., 1997; Whitaker, 1999; Quintard and Whitaker, 2000; Aguilar-Madera et al., 2011). At this point, the non-linear contribution of the temperature deviations in the reaction rate has been eliminated and can be expressed in macroscopic quantities. The non-closure upscaling model for mass transport in the Eq. (12) is complete by substitution in the surface integral term of the definition of s_{rxn} , Eq. (30), which can be expressed as

$$\frac{1}{V_\beta} \int_{\mathcal{A}_{\beta\sigma}} s_{rxn} dA = k_{(T_\sigma)^\sigma} a_v \varepsilon_\beta^{-1} \left(\omega_1 \langle C_{A\beta} \rangle^\beta + \frac{\omega_2}{\mathcal{A}_{\beta\sigma}} \int_{\mathcal{A}_{\beta\sigma}} \tilde{c}_{A\beta} dA \right) \quad (33)$$

Moreover, in the non-closure upscaling model for heat transport, Eq. (18) and Eq.(19), the surface integrals at $\mathcal{A}_{\beta\sigma}$ can be related by the heat flux boundary condition, Eq. (5c) as

$$\frac{1}{V} \int_{\mathcal{A}_{\beta\sigma}} \mathbf{n}_{\beta\sigma} \cdot k_\beta \nabla T_\beta dA = \frac{1}{V} \int_{\mathcal{A}_{\beta\sigma}} \mathbf{n}_{\beta\sigma} \cdot k_\sigma \nabla T_\sigma dA + \langle s_{rxn} H \rangle \quad (34)$$

where $\langle s_{rxn} H \rangle$, as will be shown in the next section, is defined according to a first-order effective reaction rate. At this point, the non-linear contributions of the deviation variables have been eliminated from the governing equations, and closure problems can be solved. For brevity, the details related to statements and solutions to the closure problems can be reviewed for mass and heat transport in the Appendix B; here, we only present the formal solution as

$$\tilde{c}_{A\beta} = \mathbf{f}_\beta \cdot \nabla \langle C_{A\beta} \rangle^\beta + \mathbf{g}_\beta \langle C_{A\beta} \rangle^\beta \quad (35a)$$

$$\tilde{T}_\beta = \mathbf{b}_{\beta\beta} \cdot \nabla \langle T_\beta \rangle^\beta + \mathbf{b}_{\beta\sigma} \cdot \nabla \langle T_\sigma \rangle^\sigma - s_\beta (\langle T_\beta \rangle^\beta - \langle T_\sigma \rangle^\sigma) + r_\beta q_{rxn} \quad (35b)$$

$$\tilde{T}_\sigma = \mathbf{b}_{\sigma\beta} \cdot \nabla \langle T_\beta \rangle^\beta + \mathbf{b}_{\sigma\sigma} \cdot \nabla \langle T_\sigma \rangle^\sigma + s_\sigma (\langle T_\sigma \rangle^\sigma - \langle T_\beta \rangle^\beta) + r_\sigma q_{rxn} \quad (35c)$$

The vector \mathbf{b}_β and scalar \mathbf{g}_β are the closure variables for mass transport and the vectors $\mathbf{b}_{\beta\beta}$, $\mathbf{b}_{\beta\sigma}$, $\mathbf{b}_{\sigma\beta}$, $\mathbf{b}_{\sigma\sigma}$ and scalars, s_β , s_σ , r_β and r_σ are the corresponding closure variables for heat transport. Here $q_{rxn} = \langle s_{rxn} H \rangle$ is the averaging heat source due to surface chemical reaction.

Before moving to the next section, it is essential to emphasize that the mathematical treatment present in this work to find the appropriate reaction rate expression, in terms of average temperatures and deviation concentration, was performed for a simple first-order reaction and direct reaction kinetics. However, in the catalytic intensified process, the reactive system inside the catalyst layers involve multiphase, and multicomponent reversible reactions and diverse kinetic sequences, as mentioned above. The assumptions and restrictions on which the upscaled model is

derived in this section limit its applicability to this type of complex system and are valid for analyzing liquid-phase reactions in the catalytic porous medium of the reactive zone of intensified systems that meet these characteristics. Nevertheless, the strategy approach presented here is a starting point that could be extended to include these complexities, as mentioned above, to modeling accurate, more realistic reactive regions in the intensified catalytic process.

4. Upscaling model

In this section, we present the closed upscaling model that describes the transfer of mass and heat transport in the porous catalyst layer in the reactive region of the catalytic packing. The close upscaling mass transport equation is obtained by substituting Eq. (35a) into the surface integrals of Eq. 12, to give

$$\varepsilon_\beta \frac{\partial \langle C_{A\beta} \rangle^\beta}{\partial t} + \nabla \cdot (\varepsilon_\beta \langle \mathbf{v}_\beta \rangle^\beta \langle C_{A\beta} \rangle^\beta) = \nabla \cdot (\varepsilon_\beta \mathbf{D}_\beta^* \cdot \nabla \langle C_{A\beta} \rangle^\beta) - a_v k_{eff}^* \langle C_{A\beta} \rangle^\beta \quad (36)$$

which is expressed in terms of the total dispersion \mathbf{D}_β^* , and the effective reaction rate coefficient, k_{eff}^* , which are defined as

$$\mathbf{D}_\beta^* = \mathcal{D}_\beta \left(\mathbf{I} + \frac{1}{\mathcal{V}_{\beta\sigma}} \int_{\mathcal{A}_{\beta\sigma}} \mathbf{n}_{\beta\sigma} \mathbf{f}_\beta dA \right) - \langle \mathbf{f}_\beta \tilde{\mathbf{v}}_\beta \rangle^\beta \quad (37)$$

$$k_{eff}^* = k_{(T_\sigma)^\sigma} \left(\omega_1 + \frac{\omega_2}{\mathcal{A}_{\beta\sigma}} \int_{\mathcal{A}_{\beta\sigma}} \mathbf{g}_\beta dA \right) \quad (38)$$

The total dispersion encompasses the diffusion and hydrodynamic dispersion effects in the first and second terms. Here we use a superscript * to indicate that they contain terms generated from convection, which is more evident for total dispersion; for the effective reaction rate coefficient, and the convection comes from the associate closure problem (see B). The upscaled mass and heat transfer equations are related by a *macroscopic Arrhenius* expression, Eq. (38). As is written in the Eq.(31), $k_{(T_\sigma)^\sigma}$ depends by the imposition that the average temperature of the catalytic solid $\langle T_\sigma \rangle^\sigma$ yields for the first-order surface reaction. This form of expression is novel in that it allows us to link the mass and heat transport equations by defining the reaction rate with the average temperature of the solid phase. As will be discussed later, the form of the upscaled heat transport model also includes this definition of the effective reaction coefficient. Otherwise, the values of the ω_1 and ω_2 , as mentioned before and shown in their definitions, Eq.(32), depend on complex relations of average temperatures; an order-of-magnitude analysis could provide the significance of these relationships. We can assume the complex relations can discard as following: $1 \gg \text{OC}_2 (\langle T_\sigma \rangle^\sigma, \langle T_\beta \rangle^\beta)$ and $\omega_2 \gg \text{OC}_1 (\langle T_\sigma \rangle^\sigma, \langle T_\beta \rangle^\beta)$ as consequence $\omega_2 \approx 1$ and $\omega_1 \approx 1$. The above results in the relation between macroscopic mass and heat transfer given by the effective reaction rate: $k_{eff}^* = k_{(T_\sigma)^\sigma} \left(1 + \frac{1}{\mathcal{A}_{\beta\sigma}} \int_{\mathcal{A}_{\beta\sigma}} \mathbf{g}_\beta dA \right)$. In the case of isothermal case we can write $k_{(T_\sigma)^\sigma} = k$ and the upscaling model for mass transfer are in correspondence with those derived previously (Valdés-Parada et al., 2011; Valdés-Parada et al., 2020).

At this stage, the closure of the upscaling mass transport model is completed through the prediction of the effective coefficients. As mentioned above, these coefficients are calculated using unit cells representative of the catalytic porous medium. According to the VAM, these unit cells can be as complex and capture the essential microscopic characteristics of the reactive transport process. The unit cells work as a representation of the catalytic porous medium,

presented in the reactive zone in the catalytic column. They could be used subsequently in design analysis to improve the structural characteristics of the catalytic intensification process (Wang et al., 2017). In the particular case of this work, the analysis of the unit cell's microstructure effects is convenient because the reaction occurs on the surface of the particles. In the literature, various geometries in 2D and 3D have been used to represent the structure of porous media in mass and heat transport; which includes in-line squares and cubes (Valdes-Parada and Alvarez-Ramirez, 2010; Valdés-Parada et al., 2017), in line and staggered arrangements of circles and spheres (Porter et al., 2010; Guo et al., 2015) and complex structures of random circles and spheres (Yan and Li, 2017).

In this work, the computations of effective coefficients are performed by the solution of the associated boundary-value problem of the closure variable of f_β and g_β . The solution fields of the closure variable depend upon microscopic properties, the heterogeneous reaction rate coefficient, and molecular diffusion. The asymmetric behavior is due to the sources located on the interface of the corresponding closure problem; see B. We need to solve the momentum transport equations (i.e. Navier Stokes equations) to obtain the velocity field for the unit cells to include the convective contribution on the effective coefficients as detailed in B. The unit cells are those employed previously to obtain the permeability coefficients: circles (2D) and spheres (3D) obstacles, which represent the catalytic pellet, see Fig. 1. To carry out the closure problem solution and the subsequent calculation of effective coefficients, we use the finite element solver COMSOL Multiphysics using the adaptive mesh refinements to guarantee consistency and independence in the numerical results. Examples of the numerical dimensionless solution field of the closure variables are shown in Fig. 2 considering a longitudinal velocity (i.e., in the direction $-x$) across the unit cell.

The result of predictions of the effective coefficients, D_β^* and k_{eff}^* are shown in Fig. 3 for variations of porosity of the catalytic packed, the mass dispersion Péclet number and Thiele modulus, write as

$$Pe_\beta = \frac{\langle v_\beta \rangle^\beta \ell_c}{\mathcal{D}_\beta}, \quad \varphi = \sqrt{\frac{k_{(T\sigma)} \ell_c}{\mathcal{D}_\beta}} \quad (39)$$

where $\langle v_\beta \rangle^\beta = \|\langle \mathbf{v}_\beta \rangle^\beta\|$ is the magnitude of the velocity. As transport interpretation, these parameters characterize the flow pattern and the reaction rate influence of the surface reaction on the effective coefficients, respectively. The Fig. 3 (a) shows the variation of

the longitudinal dispersion coefficient, $D_{\beta,xx}^*$, with the Thiele number, considering a low velocity pattern (i.e. $Pe_\beta = 10^{-3}$) in the catalyst layer. It is observed that the effect of the chemical reaction increases as the φ number increases to similar values, independent of the porosity and geometry of the unit cell, and when the Thiele moduli become large (i.e. $\varphi > 10$), the values of dispersion $D_{\beta,xx}^* \rightarrow \mathcal{D}_\beta$. These results are consistent with those previously shown in the literature for analogous mass transport (Valdes-Parada and Alvarez-Ramirez, 2010; Qiu et al., 2017). The results clearly show the influence of the porosity and unit cell geometry (i.e. dimension effect) on $D_{\beta,xx}^*/\mathcal{D}_\beta$, to have a more quantitative perspective of this difference, we define the following expression the percent of the difference of the effective dispersion coefficient as

$$\% \text{Difference} = \frac{|D_{3D}^* - D_{2D}^*|}{D_{3D}^*} \times 100\% \quad (40)$$

In general, as is shown in Fig. 3 (b), there are appreciable differences between the calculated values of the dispersion coefficients using 2D and 3D unit cells, the magnitude of which these differences increases with the decreases of the Thiele number and porosity, reaching values of a maximum of 15% for $\varepsilon_\beta = 0.5$. Therefore, it can be stated that the effects of unit cell geometry of the packed bed become important when the Thiele numbers become small (i.e. $\varphi \leq 10^{-3}$). Fig. 3 shows the effect of more complex situations associated with the flow pattern in the unit cell model. In Fig. 3 (c) and (d) we plot the dependence of both, longitudinal and transverse components of the dispersion coefficient with the Peclet number for values of the Thiele number with different orders of magnitude (i.e. $\varphi = 10^{-1}, = 10^0, = 10^1$) and fixed porosity ($\varepsilon_\beta = 0.5$). These coefficients feature the usual profiles of dispersion coefficients, i.e. pure diffusion at low Peclet numbers Pe_β , a transition regime, and asymptotic dependence ($\sim Pe_\beta^n$) for large Peclet.

The profiles of the longitudinal and transverse dispersion coefficient show the same trend for the results of 2D and 3D unit cells for the range of Pe_β values considered here. We notice in Fig. 3 (c) that an increment in the Thiele modulus leads to a lightly increase in the values of longitudinal dispersion tensor, which is more evident in the corresponding transverse component, Fig. 3 (d). In the case of the dependence of the dispersion coefficient on the Peclet number, the effect of the 2D and 3D unit cell geometry is particularly noticeable for most of the Pe_β values, as is seen in Fig. 3 (e) - (f). In general, the percentages are about 10% ($\varphi > 10^0$) for

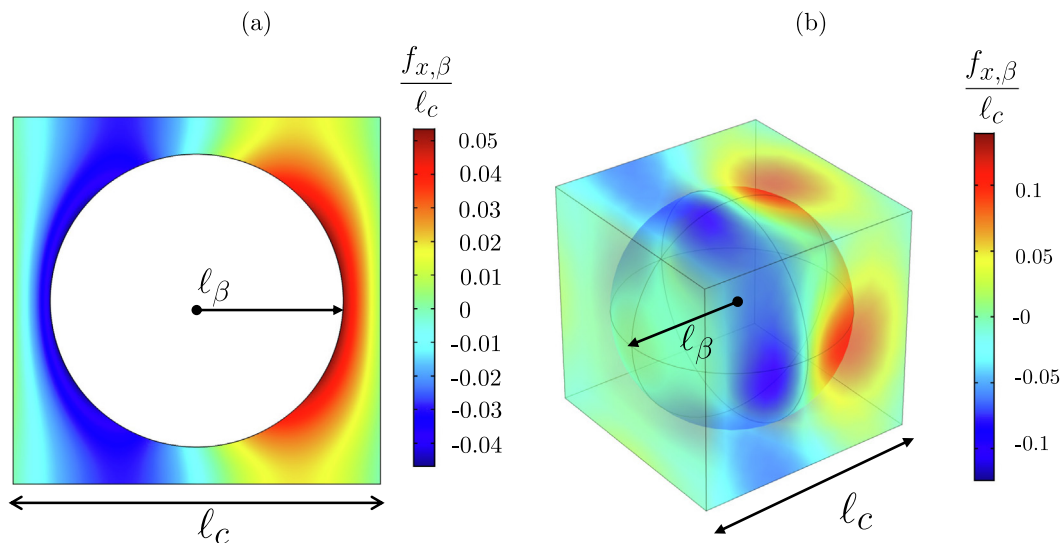


Fig. 2. (a) Solution profile of $f_{x,\beta}/\ell_c$ for periodic unit cell 2D y 3D. $\varepsilon_\beta = 0.5$ and $Pe_\beta = 10^1$.

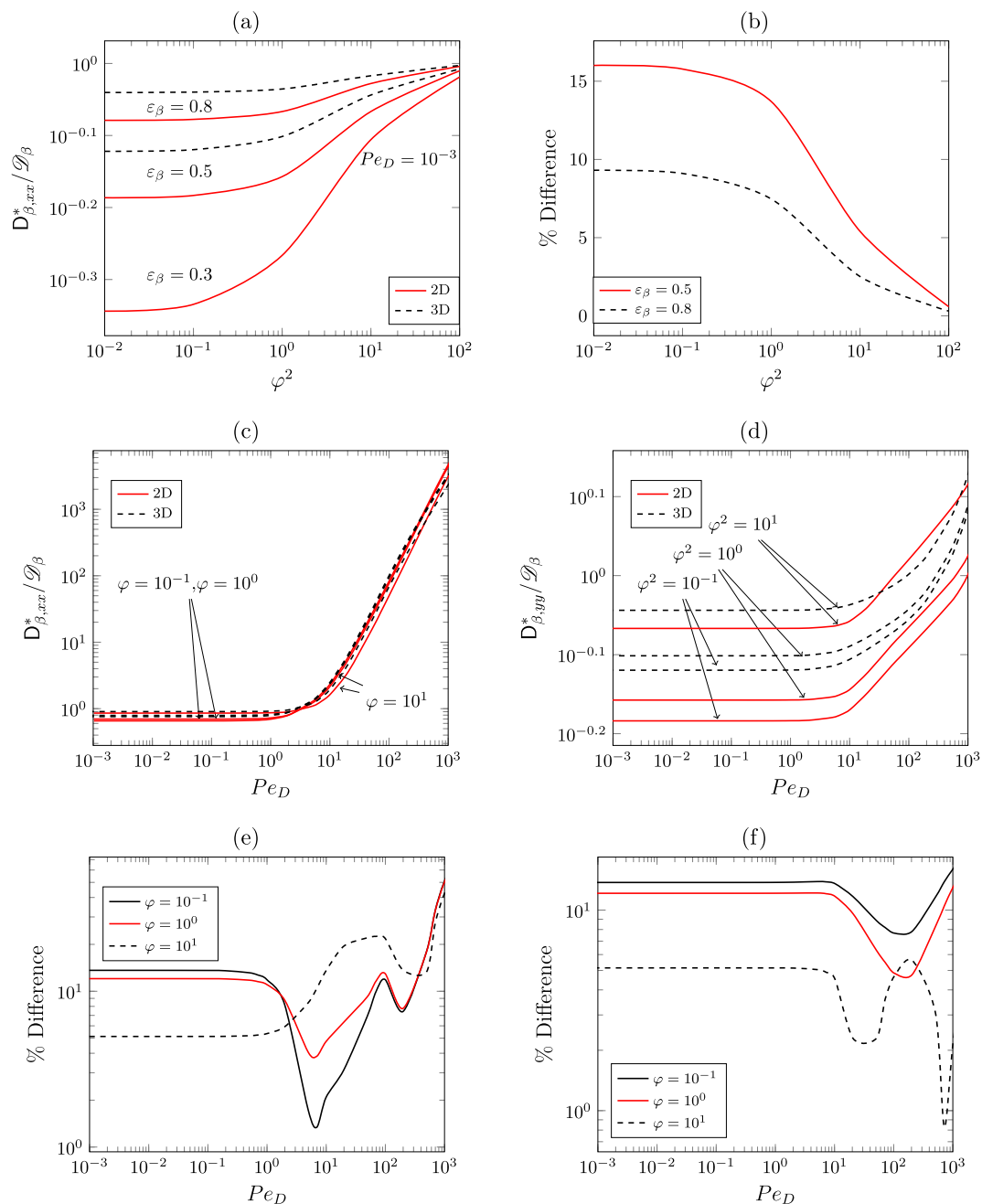


Fig. 3. (a) Effect of the porosity in the longitudinal dispersion coefficient as functions of Thiele moduli with $Pe_\mathcal{D} = 10^{-1}$. (b) Percentage difference between 2D and 3D unit cells in the longitudinal dispersion coefficient. (c) Longitudinal and (d) transverse dispersion coefficients as functions of the particle Péclet number, Pe_D and Thiele moduli. Percentage difference with the variations of Thiele moduli of the (e) longitudinal and (f) transverse dispersion coefficient. The porosity is $\varepsilon_\beta = 0.5$.

$Pe_\mathcal{D} < 10^0$ reaching higher percentages for larger values of the Péclet number ($Pe_\mathcal{D} = 10^2$). The erratic behavior shown in the percentage differences between the values $Pe_\mathcal{D} = 10^0 - 10^2$ can be attributed to the transition from diffusive to convective effects in the respective unit cells (Valdés-Parada et al., 2017).

In the proposed mass transport upscaling model, the influence of the surface reaction that occurs in the catalytic bed of the reactive zone can be characterized through predictions of the effective reaction rate coefficient, k_{eff}^* . As indicated by its definition, Eq. (38), this coefficient links the chemical kinetics via the Arrhenius-type expression and the surface integral of the closure variables, which we can consider as an upscaling correction. The predictions of the effective rate coefficient, dependent on the Thiele number for var-

ious values of the Péclet numbers and fixed porosity of $\varepsilon_\beta = 0.5$, are shown in Fig. 4 using 2D unit cells. As expected, for $\varphi < 10^0$, the effective reaction rate coefficient $k_{eff}^* \rightarrow k_{(T\sigma)}^\sigma$ and the values of the reaction rate coefficient decreases as φ increases with the influence of the magnitude of the convection, $Pe_\mathcal{D} > 10^1$. If the ratio $k_{eff}^*/k_{(T\sigma)}^\sigma$ is defined as an effectiveness factor η (Wood et al., 2007), it would correspond only to the surface integral of the closure variables associated with the source of the surface chemical reaction, Eq. (38). Thus there is a relationship between a reaction parameter at the catalytic bed scale with one associated with the reaction at the surface of the catalytic particle; analogous to the classical interpretation of *intrinsic velocity* reaction (Chemical Reactor Analysis and Design, 2010). The above could therefore involve

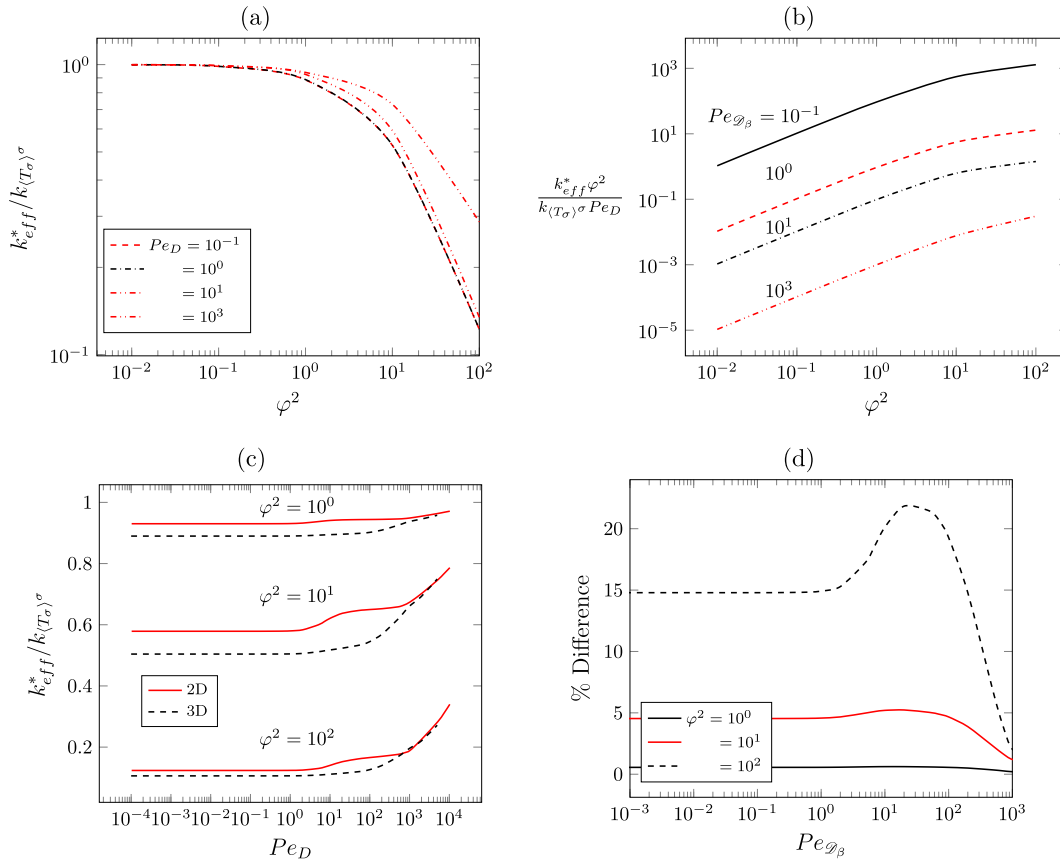


Fig. 4. (a) Dependence of the effective reaction coefficient with φ and $Pe_{\mathcal{D}}$. (b) Dependence of the normalized effective reaction with the Thiele module with φ using 2D unit cell. (c) Comparison of the effective reaction coefficient using 2D and 3D unit cells. (d) Percentage difference 2D and 3D of effective rate coefficient. The porosity is $\varepsilon_{\beta} = 0.5$.

the predictive ability of an effectiveness factor in dependence on φ , $Pe_{\mathcal{D}}$, and the geometry of the unit cell. In addition, we can reinterpret this relationship as a scaling factor that considers the surface kinetic conditions involving the convective transport of mass in catalytic porous media. We notice that the effective rate coefficient is not the same as the kinetic constant for the heterogeneous reaction set out in this work, but it is a function of a semi-local Thiele modulus due $k_{(T_s)\sigma}$ is defined by the averaging temperature of the solid phase. In Fig. 4 (b), we plot the normalized effective reaction rate coefficient with the φ and $Pe_{\mathcal{D}}$ to visualize the effect of the velocity flow and the heterogeneous reaction for a 2D unit cell with the Péclet number, values are ranging in four magnitude orders. We observe that the effect of the dispersion transport in reasons for the effective rate coefficient is not the same as the kinetic *constant* for the heterogeneous surface reaction, but it is a function of the local Thiele modulus in the catalytic bed.

To finalize with mass transport coefficients associated with the upscaling model development in this work and to point out the effect of the unit cell geometry on the effective reaction coefficient, in Fig. 4(c), we examine the dependence of the rate coefficient factor with various values of $Pe_{\mathcal{D}}$ for several values of φ with differences in magnitude order. More evident in these results is the effect of the chemical reaction on the effective reaction coefficient where k_{eff}^* decreases as the φ decreases, with appreciable differences given the unit cell used in the calculation of the predictions. To gain further insight into the influence of the representative cell geometry of the catalytic bed, Fig. 4 (d) shows the percentage differences between the predicted values of the $k_{eff,2D}^*$ and $k_{eff,3D}^*$ coefficients, analogous to Eq. (40). These results show that the percentage error increases with increasing magnitude of φ , remaining

relatively the same value for $Pe_{\mathcal{D}} < 1$ at a value less than 17%, increasing to a maximum of 35% in the range of $Pe_{\mathcal{D}} = 10^0 - 10^2$, to become practically independent of the unit cell geometry at values of $Pe_{\mathcal{D}} > 10^3$. This rapid increase can be explained by the fact that the transition from diffusive to convective process, influenced by the surface reaction, occurs at these values of Péclet. It is worth pointing out that the predictions, in the values of $Pe_{\mathcal{D}}$, cover only the non-inertial range in the simulations for the catalytic bed in both 2D and 3D unit cells, on these inertial effects may be a significant increase in the effective rate coefficient for first-order heterogeneous reaction in the catalytic bed and this motives further study.

To complement the upscaling model for the catalytic packed is necessary to derive the corresponding macroscopic equations of heat transfer in the fluid and solid particle and predict the associated effective coefficients. We derive the macroscopic equation for heat transfer by the substitution of Eqs. (35) (b) - (c) into Eqs. 13,14 to obtain the following govern equations for fluid phase and the catalytic solid, respectively

$$\begin{aligned}
 \varepsilon_{\beta}(\rho c_p)_{\beta} \frac{\partial \langle T_{\beta} \rangle^{\beta}}{\partial t} + (\rho c_p)_{\beta} \nabla \cdot (\langle \mathbf{v}_{\beta} \rangle^{\beta} \langle T_{\beta} \rangle^{\beta}) \\
 = (\rho c_p)_{\beta} \nabla \cdot [\mathbf{u}_{\beta\beta}^* \langle T_{\beta} \rangle^{\beta} + \mathbf{u}_{\beta\sigma}^* \langle T_{\sigma} \rangle^{\sigma}] + \nabla \\
 \cdot [\mathbf{K}_{\beta\beta}^* \nabla \cdot \langle T_{\beta} \rangle^{\beta} + \mathbf{K}_{\beta\sigma}^* \nabla \cdot \langle T_{\sigma} \rangle^{\sigma}] - a_v h (\langle T_{\beta} \rangle^{\beta} - \langle T_{\sigma} \rangle^{\sigma}) \\
 - \xi_{\beta} \langle q_{rxn} \rangle
 \end{aligned} \quad (41)$$

$$\begin{aligned} \varepsilon_\sigma (\rho c_p)_\sigma \frac{\partial \langle T_\sigma \rangle^\sigma}{\partial t} &= (\rho c_p)_\beta \nabla \cdot \left[\mathbf{u}_{\sigma\beta} \langle T_\beta \rangle^\beta + \mathbf{u}_{\sigma\sigma} \langle T_\sigma \rangle^\sigma \right] + \nabla \\ &\cdot \left[\mathbf{K}_{\sigma\beta} \nabla \cdot \langle T_\beta \rangle^\beta + \mathbf{K}_{\sigma\sigma} \nabla \cdot \langle T_\sigma \rangle^\sigma \right] \\ &- a_v h \left(\langle T_\sigma \rangle^\sigma - \langle T_\beta \rangle^\beta \right) + \xi_\sigma \langle q_{rxn} \rangle \end{aligned} \quad (42)$$

These expressions agree with previous formulations for dispersive heat transport for the two-equation model for heat transfer (Ochoa-Tapia and Whitaker, 1997; Quintard et al., 1997; Quintard and Whitaker, 2000). The presence of a heat source due to the surface reaction on the catalytic particle means that Eqs. 41,42 involve the additional last terms, which allows us to relate it to the macroscopic mass transport equation (Eq. 36), previously derived. These equations include several effective heat transfer coefficients defined in terms of the closure variables associated with the temperature. The effective coefficient includes the heat dispersion tensors, for example the $\mathbf{K}_{\beta\beta}^*$ and $\mathbf{K}_{\sigma\sigma}$ are written as

$$\mathbf{K}_{\beta\beta}^* = k_\beta \left(\varepsilon_\beta \mathbf{I} + \frac{1}{\mathcal{V}} \int_{\mathcal{A}_{\beta\sigma}} \mathbf{n}_{\beta\sigma} \mathbf{b}_{\beta\beta} dA \right) - (\rho c_p)_\beta \langle \tilde{\mathbf{v}}_\beta \mathbf{b}_{\beta\beta} \rangle \quad (43)$$

$$\mathbf{K}_{\sigma\sigma} = k_\sigma \left(\varepsilon_\sigma \mathbf{I} + \frac{1}{\mathcal{V}} \int_{\mathcal{A}_{\sigma\beta}} \mathbf{n}_{\sigma\beta} \mathbf{b}_{\sigma\sigma} dA \right) \quad (44)$$

Similar expressions can be written for the other dispersion coefficients for the rest of the effective coefficients, as presented in B. In the case of the heat transport equation for the fluid, the terms with $\mathbf{u}_{\beta,m}$, $m = \beta, \sigma$ represent a velocity vector which results from the conduction and dispersion in the fluid; whereas the alike-convective terms $(\rho c_p)_\beta \nabla \cdot \left[\mathbf{u}_{\beta m} \langle T_m \rangle^m \right]$ arising from the interactions fluid–solid phases and $a_v h$ is the interfacial heat transport. As we can notice, analogous effective coefficients are present in the Eq. (42) for the solid phase equation, remarking that we have used * superscript to distinguish the effective coefficients that contain terms generated by convection. In addition, the presence of convective-like coefficients in the Eq. (42), despite evidence that no heat convection transport in the solid phase, is attributed to the interaction between transport and effective conduction at the pore-level (Quintard et al., 1997). Finally, the terms attributed to the average surface source due to the reaction are defined in terms of the effective reaction rate coefficient and the average concentration according to

$$\langle q_{rxn} \rangle = k_{eff}^* \langle c_{A_\beta} \rangle^\beta \times H \quad (45)$$

This term in the macroscopic equations of heat transport contrasts with the previous works (Quintard et al., 1997; Quintard and Whitaker, 2000; Yang et al., 2015a), in which the non-linear contributions of the deviation quantities were not discarded explicitly from the macroscopic heat transport equation. As matter of fact, the definition of $\langle q_{rxn} \rangle$ given in the Eq. (45) indicate clearly the relation with the effective reaction rate coefficient, k_{eff}^* , the macroscopic concentration, $\langle c_{A_\beta} \rangle^\beta$, and the heat reaction, H ; this corresponds to the original contributions of this work. As previously discussed, k_{eff}^* is calculated from the solution of the transport closure problem for mass and the corresponding value $k_{(T_\sigma)\sigma}$. Therefore, the non-linear relation of the Arrhenius-type Equation, Eq. (40) generates both upscaled models for mass and heat transport related to each other. In addition, the effective coefficient that multiplies this term, ξ_β and ξ_σ , can interpret as the volume distribution coefficients for heat produced due to the reaction in the interface between the catalytic solid and fluid phase. They are defined as

$$\begin{aligned} \xi_\beta &= \frac{k_\beta}{\mathcal{A}_{\beta\sigma}} \int_{\mathcal{A}_{\beta\sigma}} \mathbf{n}_{\beta\sigma} \cdot \nabla r_\beta dA, \quad \xi_\sigma \\ &= \frac{k_\sigma}{\mathcal{A}_{\beta\sigma}} \int_{\mathcal{A}_{\sigma\beta}} \mathbf{n}_{\sigma\beta} \cdot \nabla r_\sigma dA, \quad \xi_\beta + \xi_\sigma = 1 \end{aligned} \quad (46)$$

Thus, the upscaling model for heat transfer is completed by calculating the effective coefficients obtained under the same solution scheme presented previously for mass transport. These predictions consist of the solution profiles of the closure problems in 2D and 3D unit cells under different velocity rates and their subsequent substitution in the explicit definitions of these coefficients. Examples of the solution profiles are presented in B. These predictions are made for various values of thermal Péclet number and conductivity ratios,

$$Pe_T = (\rho c_p)_\beta \frac{\langle v_\beta \rangle^\beta \ell_c}{k_\beta}, \quad \kappa = k_\beta / k_\sigma \quad (47)$$

The results of the longitudinal and transversal component of the thermal dispersion coefficient of β -phase, $K_{xx,\beta\beta}^*$ and $K_{yy,\beta\beta}^*$, is shown in Fig. 5 (a) and (b) as a function of Peclet number and for different porosity and dimension. The effective coefficients exhibit similar profiles to those shown previously for mass dispersion, Fig. 3 (c) and (d), and as expected, the values of the transverse component are much smaller than the longitudinal. Indeed, these figures show qualitative differences in the values of the thermal dispersion coefficients that depend on the geometry of the unit cell, which decreases with increasing porosity. This influence is evident by analyzing the percentage difference of these values of longitudinal and transverse dispersion shown in Fig. 5 (c) and (d), respectively. It is observed that the percentage difference for the longitudinal component does not exceed 10% for $Pe_T < 10^0$, increasing rapidly to values greater than 100% for $Pe_T > 10^2$. For the transverse component, the differences are less than 10%. As in the case of mass transfer, the influence of the unit cell model representative of the catalytic bed should be considered in the predictions of the effective coefficients, mainly for large Pe_T . The other thermal coefficients component are presented in Fig. 5 (e) and (f), and similar comments can be drawn. These results indicate values of $K_{xx,\sigma\sigma}$ are smaller than the β -phase and present an opposite profile concerning the dependence on porosity. On the other hand, Fig. 5 shows that the coupling tensors $K_{xx,\beta\sigma}^*$ and $K_{xx,\sigma\beta}$, for range values of Pe_T , are very small compared to the principal coefficients $K_{xx,\beta\beta}^*$ and $K_{xx,\sigma\sigma}$.

To analyze the dependence of the effective coefficients on the characteristic thermal conductivities ratio, the dependence of thermal coefficients as a function of κ for various order magnitudes of Pe_T is presented in Fig. 6 by fixing $\varepsilon_\beta = 0.5$. In general, the influence on the effective thermal coefficients with velocity can be considered negligible for $Pe_T < 10^0$ for the whole range of κ , turning relative relevant for large values of the Péclet number. The Fig. 6 (a) shows the influence of κ in the $K_{xx,\beta\beta}^*$ is important in the range of $10^{-1} < \kappa < 10^1$, outside these values we observe κ does not affect greatly and approaches a constant values. These profiles show that the value of $K_{xx,\beta\beta}^*$ increases for $Pe_T \leq 10^0$ and oppositely for $Pe_T > 10^0$, denoting the influence of the velocity rate on this coefficient. In the case of the coefficient for the solid phase, $K_{xx,\sigma\sigma}^*$, their value increases in an asymptotic trend towards a constant value slightly influenced by the Pe_T . The functionality of volume interfacial heat transfer, $a_v h$, with the ratio conductivities, is shown in Fig. 6 (c). The profiles shown by this interfacial coefficient are similar to those described previously, with magnitudes of the coefficient values much larger than those corresponding to $K_{xx,\sigma\sigma}^*$. The no dependency shown in Fig. 6 (c) with Pe_T , between $\kappa < 10^0$ of

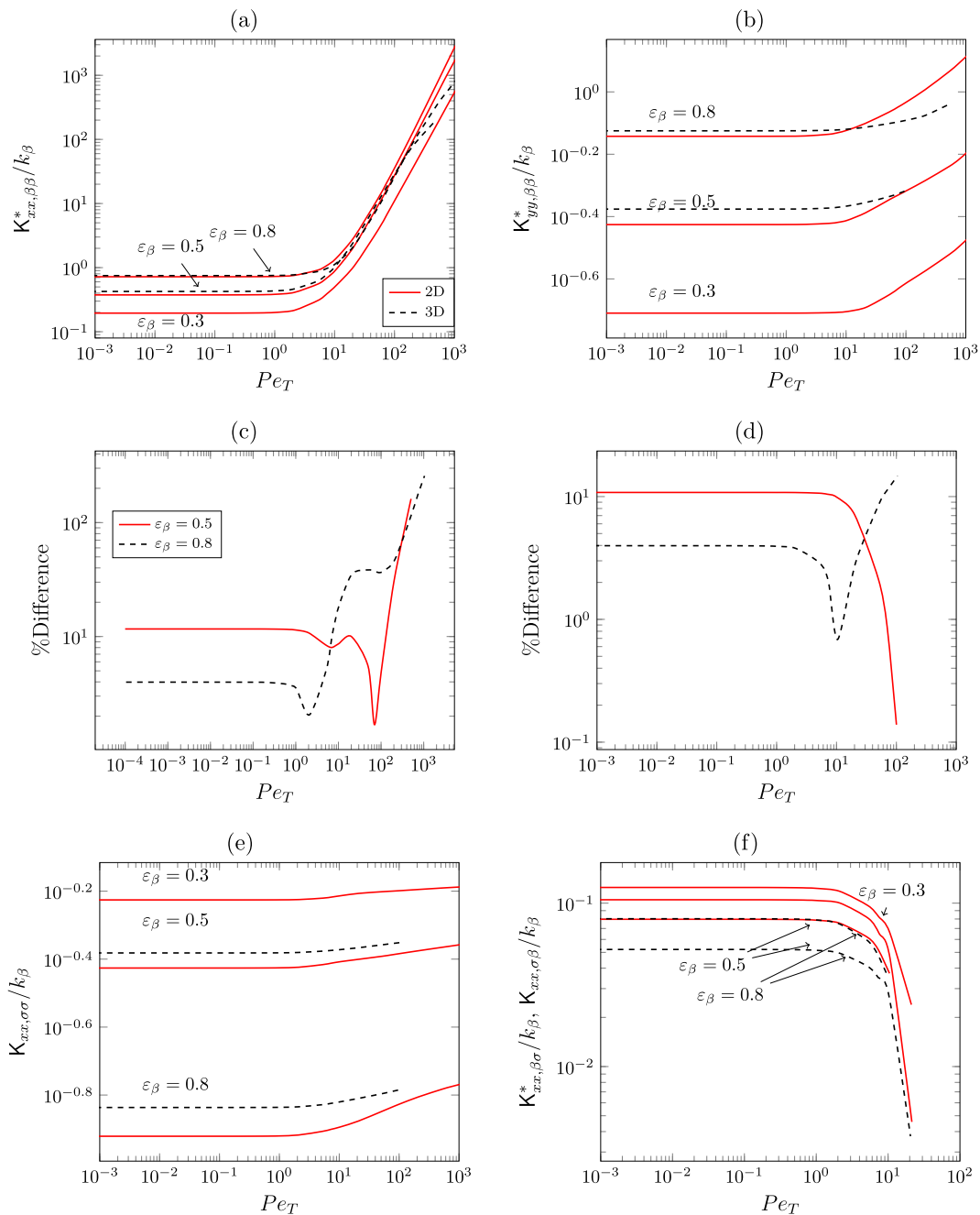


Fig. 5. (a) Longitudinal and (b) transverse thermal dispersion coefficient for fluid phase. (c) and (d) are Percentage difference using 2D and 3D unit cells. (f) and (g) are Longitudinal co-dispersion coefficient for phases interactions.

$a_p h$, is attributed to the dominance of heat resistance of the catalytic solid. With respect to the coefficients associated with the convective-like term, $u_{x,\beta,m}^*$ and $u_{x,\sigma,m}$, $m = \sigma, \beta$ to keep the document brief, these results are shown in B. It is pointed out that, like the results shown here, the values present a clear dependence in their magnitude with the velocity rate as a function of the geometry of the 2D and 3D unit cells used for their calculation. In general, these coefficients' result is consistent with the previous observations for similar 2D unit cells (Quintard et al., 1997).

Finally, we focus on the predictions of the effective coefficients associated with the heat source term due to the surface chemical reaction. For a stratified system, analytical expressions for the predictions of these effective coefficients can be found in the literature (Quintard and Whitaker, 2000). In this study, we extend the

predictions of these coefficients computed for unit cells of the catalyst particle in 2D and 3D with the novelty of analyzing the applications of the upscaling model in the catalyst layer with equal structural particles. The volume distribution coefficient ξ_β and ξ_σ as a function of thermal conductivity are plot in Fig. 8 (d). The results show that for low values of κ , i.e $\kappa \rightarrow 0$, the process the heat distribution reaction source is in the fluid phase, and $\xi_\beta \approx 1$. In opposition, when the fluid phase does not dominate the heat transfer, large values of κ , the heat source of the reaction distribution is in the catalytic solid, and $\xi_\sigma \approx 1$.

Furthermore, it is observed that the influence of κ on the value of the distribution coefficients is more significant in the interval of $10^{-1} < \kappa < 10^1$, increasing its value as Pe_T increases. Additional results, not presented here for brevity, show that a decrease in

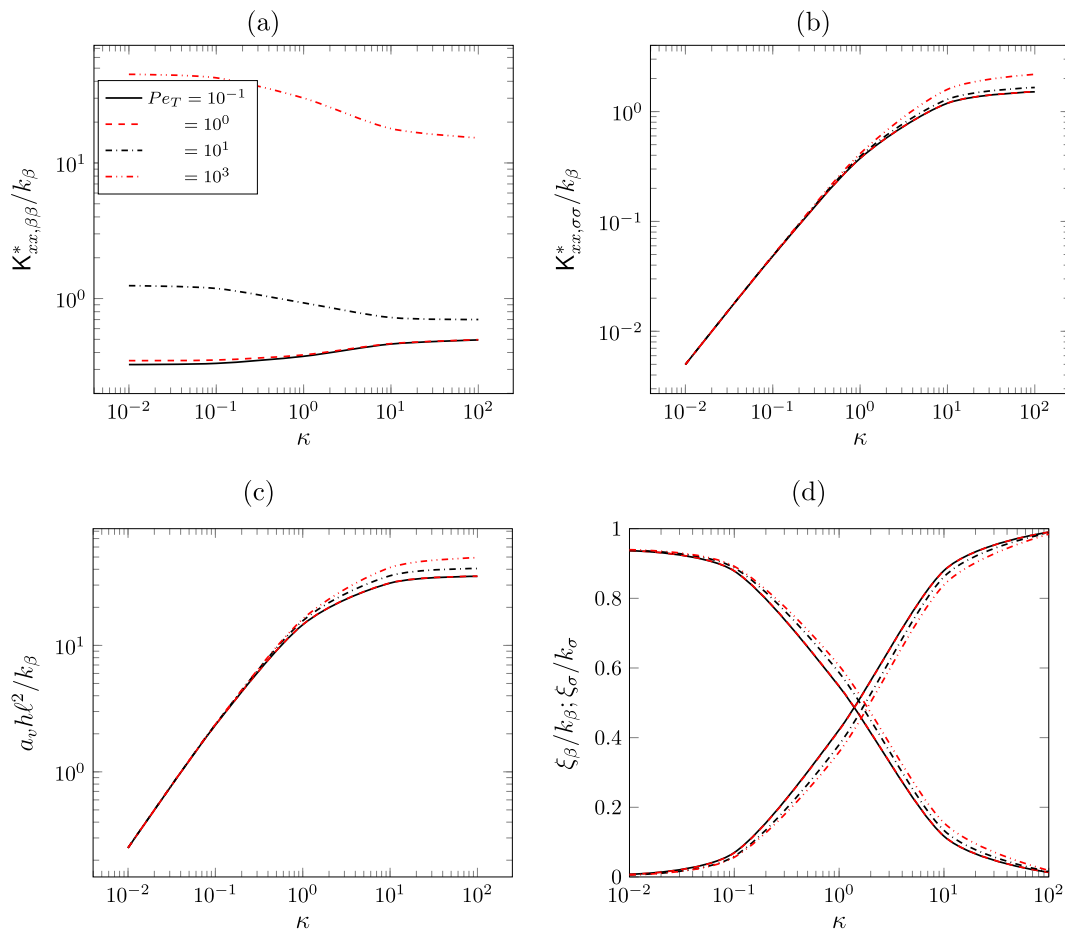


Fig. 6. (a) longitudinal thermal dispersion coefficient, (b) transverse thermal dispersion coefficient, κ , (c) volume reaction heat distribution coefficient, as a function of the thermal Péclet, Pe_T , for $\varepsilon_\beta = 0.5$.

ε_β , an increase in the surface area available to the reaction source, increases ξ_β in the range around $\kappa = 1$ with an increase; with the opposite behavior for ξ_σ . Moreover, the influence of velocity is more noticeable with decreasing porosity. Similar profiles are observed between 2D and 3D unit cells, where percentages of difference of up to 30% are presented, significantly influencing the value of the reaction volume distribution coefficient.

The relevance of computing the effective coefficients associated with mass and heat transfer are: firstly, these coefficients allow for the determination of the averaged concentration and temperature profiles at the scale of the catalyst layer, and secondly, the influence of mass and heat transport with surface reaction in the micro and macroscale description of transport on the catalyst packing. The above is based on the analysis of the appropriate microstructures of the catalyst layer, as is suggested in the multi-scale analysis of the catalytic packing process (Wang et al., 2017). In the next section, the concentration and temperature profile models have compared with the pore-scale numerical simulations to evaluate the macroscopic models developed in the previous sections.

5. Comparison of the macroscopic model with microscopic pore scale calculations

To evaluate the accuracy of the upscaling model's development in this work, in this section, we compare the averaged concentration and temperature profiles with numerical simulations carried out at the micro-scale (Direct Pore-Scale simulations, DPS) over a microscopic geometry of the catalytic packing. The comparison

with the DPS allows us to analyze the validity of the scaling laws used to describe the reaction process through the macroscopic equations of mass and heat obtained (Wood and Valdés-Parada, 2013). On the other hand, it allows us to consider that the model can be used to describe satisfactorily the reaction process that takes place in the catalyst particles packed. The microstructure model of the catalyst layer is made of the square pattern of parallel cylinders (2D) for the sake of consistency with the unit cell used in the closure problems for effective coefficient predictions. The simulation domain consists of a horizontal array in the flow direction (x -direction) made up of unit cells of dimensions $\ell_c \times \ell_c$, whose total length is $L = N \times \ell$, where N is the total number of unit cells, as sketched in Fig. 7. In general, the size of L should be selected as long as the constraint $\ell_c \ll r_0 \ll L$, at a minimum length that guarantees one order of magnitude of separation between the characteristic lengths. For the numerical simulations, the microscopic, given by Eq's. (4)–(5) and microscopic mass, Eq. (41)–(42) and heat equations are subject to the following initial and boundary conditions for the solution domain,

$$\text{at } x = 0, \quad c_A = \langle c_{A\beta} \rangle^\beta = c_{in}, \quad T_\beta = \langle T_\beta \rangle^\beta = T_{in} \quad (48a)$$

$$\text{at } x = L, \quad \frac{\partial c_A}{\partial x} = 0, \quad \frac{\partial \langle c_{A\beta} \rangle^\beta}{\partial x} = 0, \quad \frac{\partial T_\beta}{\partial x} = 0, \quad \frac{\partial \langle T_\beta \rangle^\beta}{\partial x} = 0, \quad (48b)$$

$$\text{when } t = 0 \quad c_A = \langle c_{A\beta} \rangle^\beta, \quad T_m = \langle T_m \rangle^m = T_0, \quad (m = \beta, \sigma) \quad (48c)$$

Additionally, periodic boundary conditions were imposed at the upper and lower boundaries of the array of unit cells. The velocity field is obtained from solving the Navier–Stokes equations in the

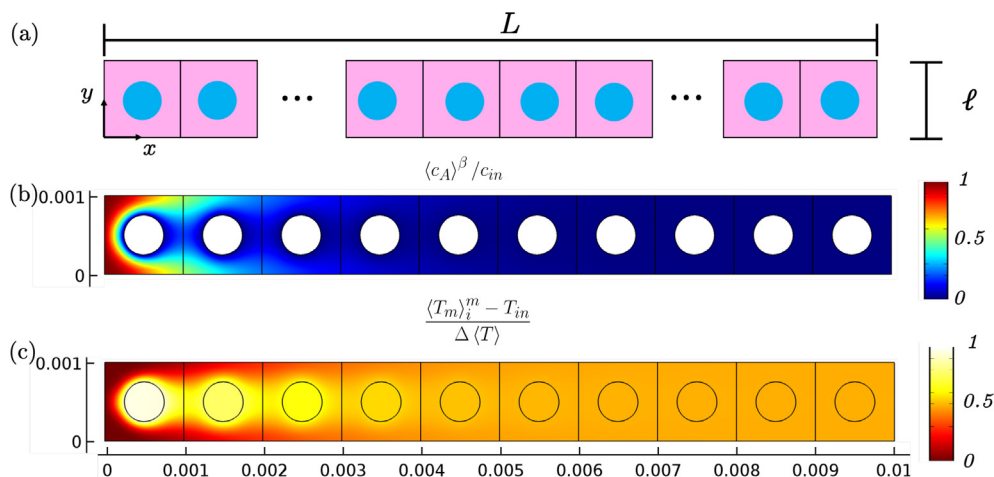


Fig. 7. (a) Simulation domain for the 2D system used to perform the pore-scale numerical simulations. (b) Dimensionless concentration DPS solution field for first unit cells of the domain. (c) dimensionless temperature DPS solution field for first unit cells of the domain. (d) dimensionless temperature DPS solution contour for first unit cells of the domain. The length of the porous medium is chosen to be maximum $L = 100\ell$ and $\varepsilon_\beta = 0.5$.

microscopic model subject to a pressure drop relative to the mass Péclet number, Pe_β . The thermal properties of the liquid and catalytic phases and the transport properties used in the numerical simulations are presented in Table 1. This Table also includes the parameters associated with the surface chemical reaction. The characterization of the surface chemical reaction is evaluated using the Thiele modulus that for the microscopic and macroscopic are defined based on the T_{in} (Eqs. (31) and (39)). We assume that it varies according to the coefficient A_0 . The effective properties in the upscale model are determined considering the properties of Table 1 and solving the closure problems, as shown in the previous section. The macroscopic equations are solved in a 1D domain with the same length, L , as the microscopic system and subject to the identical boundary conditions of DPS, Eq. (48c).

5.1. Results and Discussion

The micro and macroscale model is solved by using COMSOL Multiphysics. The independence of the number of computational elements in the numerical results is guaranteed by involving adaptive mesh refinements algorithms. Examples of the solution field of pore scale temperature and concentration are shown in Fig. 7. The average concentration and temperature profiles in both fluid and catalytic phases, of the upscaled model and DPS, for variations of the Péclet, porosity, and Thiele moduli, are shown in Fig. 6. In these figures, the results normalize with c_{in} for average concentration and the temperature difference with $\Delta\langle T \rangle = \max\langle T_\beta \rangle^\beta - \langle T_m \rangle_i^m$, $i = DPS, VAM$, for average temperatures. In general, in all the profiles shown, the predictions of the upscaled model show good agreement with those obtained via the DPS. The concentration propagates over a greater distance in the catalyst layer due to the increase in velocity rate; see Fig. 6 (a). In the case

of the temperature profile, this increase in concentration is reflected, in the input system, as an increasing value of the temperature difference associated with the solid phase, see Fig. 6 (b). These profiles show that in the macroscopic model, the reaction source is associated with the surface temperature of the catalytic solid, $\langle T_\sigma \rangle^\sigma$. On the other hand, at small values of the Péclet number and a sufficiently large distance, the differences between the catalytic solid and the fluid phase temperatures are small enough to be considered the case of *local thermal equilibrium*. The above is a reminiscent assumption for thermal analysis in porous media such as the catalyst layer.

To analyze the viability of the upscaled model to structural variations of the catalytic packing representation, Fig. 6 (c) and (d) show the temperature and concentration profiles considering variations in the porosity of the unit cell. The results present the same characteristics described previously; however, in this figure, it can be observed that the concentration and temperature profiles are less influenced by the porosity, being those of larger magnitude corresponding to the lowest porosity. This is reflected by the higher temperature difference obtained at $\varepsilon_\beta = 0.3$; see Fig. 6 (d). It is attributed to the larger surface area between the fluid and catalytic phases corresponding to this porosity and their dependency, which are associated with the effective coefficients defined in surface integrals.

For variations of the Thiele moduli, φ , that characterize the surface reaction, it can be seen in Fig. 6 (e) that the concentration profiles are practically independent with this parameter for a fixed value for Pe_β and porosity. On the other hand, appreciable differences between the temperatures of the fluid phase and the catalytic solid are observed in Fig. 6 (f), which shows that the profile predictions are more sensitive to this parameter. The largest differences are present for $\varepsilon = 10^0$, and the upscaling model under-

Table 1
Properties of solid catalyst and fluid.

	σ -phase		β -phase		
ρ	2100		0.3		kg/m ³
c_{pm}	800		1200		J/kgK
k_m	1		0.025		W/mK
	Reaction parameter				
H	391.9	kJ/mol	\mathcal{D}_β	2×10^{-8}	m/s ²
		E	8314	J/mol	

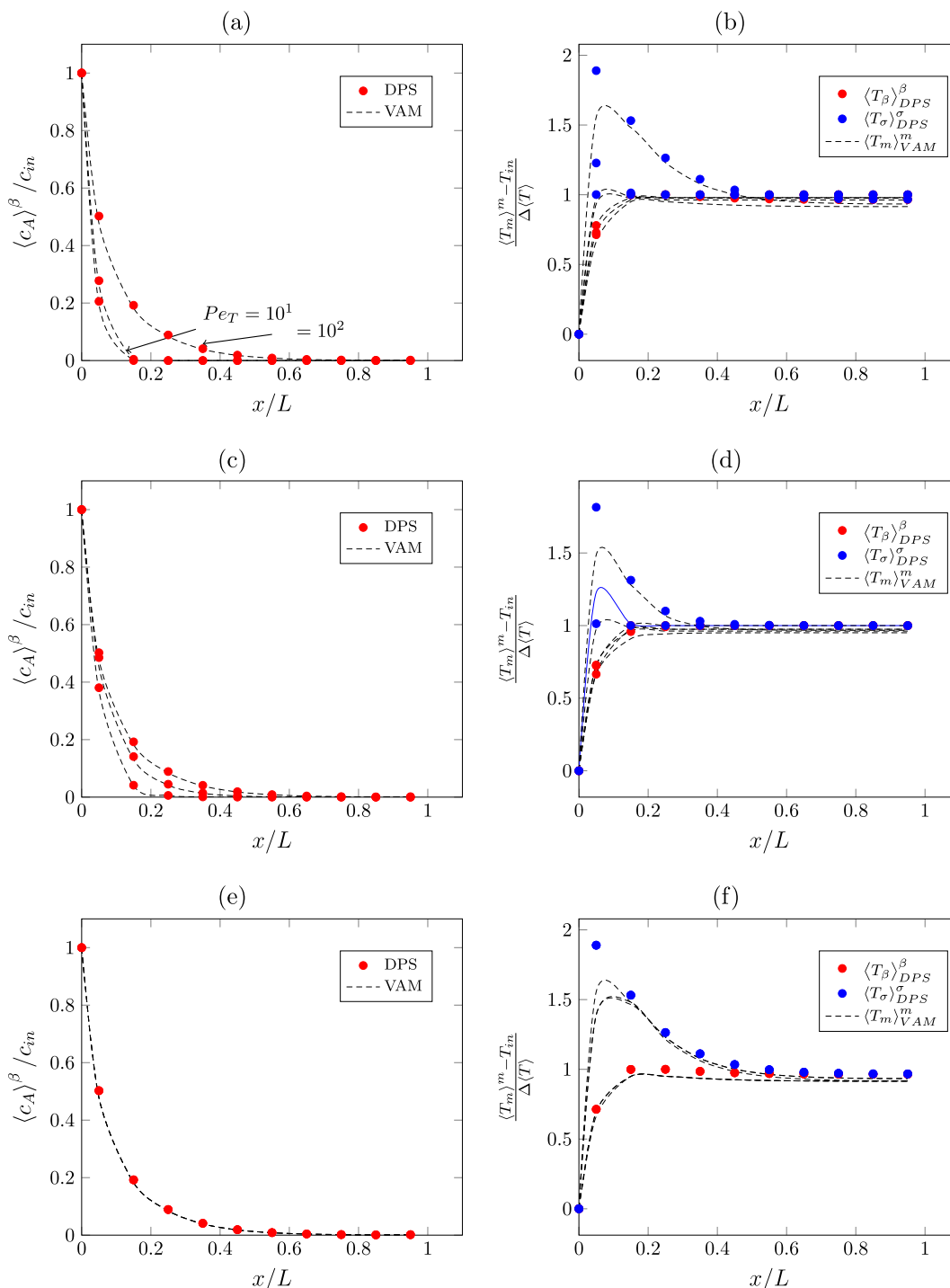


Fig. 8. Comparison of average concentration and temperature resulting from the upscaled model (VAM) and the DPS: (a)-(b) Péclet variations for $\varepsilon_\beta = 0.5$, (c)-(d) Porosity variation for $\varphi = 1$ and $Pe_\varphi = 10^1$ and (e)-(f) Thiele moduli variations for $\varepsilon_\beta = 0.5$ and $Pe_\varphi = 10^2$.

predicts the temperature profiles. This agrees with the values of k_{eff}^* performed previously, see Fig. 4 (c). It is important to remember that the reaction coefficient relates to estimates of the temperature deviations required in the upscaling process. Neglecting the higher orders in Eqs. (27) and (29) for small Thiele values could increase errors in the predictions of the effective reaction coefficient; this could explain the observed differences between the upscaled model and the DPS. This behavior is also observed for large Péclet numbers and low porosities; see Fig. 8 (b) and (d), respectively. Although the discrepancies are relatively moderate, the macro-

scopic model predicts a similar trend to DPS in temperature values and profile shape.

Concerning the comparisons between the microscopic model and the upscaled model obtained for the Pe_φ number, porosity, and φ variations, we can summarize the following comments:

- The concentration profile is adequately predicted with the upscaled model for the cases presented here. Generally, the percentage error concerning the microscopic model is less than 5%.

- In the case of the fluid and solid catalytic temperatures, the profiles of upscaled and microscopic models match well. The most significant errors are visible in the solid temperature. Mainly for the extreme parameters used to analyze the scaled model, *i.e.* large Péclet, low porosities, and small Thiele. These suggest that the effect of surface reaction and temperature deviations is associated with the effective reaction coefficient. Considering the conditions for which the temperature differences are appreciable, the possibility of a local thermal equilibrium model is discarded.
- The comparison of the upscaled and DPS models predictions shows, in general, a similar trend, demonstrating the viability of the macroscopic model obtained in terms of effective coefficients

The results show that using unit cells representative of the catalytic packing allows associating a selection scheme of suitable geometries in calculating effective coefficients. It allows us to compute the temperature and concentration profiles of the catalyst layers, including their geometric structure, in the reactive catalytic layers of the reactive column packing. Predicting the effective coefficients through the solution of the closure problems is essential in the approach proposed in this work. As mentioned in the introduction, CFD tools can be used to rigorously analyze mass-heat transfer processes with chemical reactions within catalytic layers. However, in the case of computational costs, these tools can be prohibitive, and the upscaled models developed in this work can be used to adequately predict the average temperature and concentration profiles without requiring simulation on the complex microstructure of the catalytic porous medium of the catalytic layers. Hence, the upscaled model and effective ancillary coefficients could be used as novelty surrogate input data for rigorous simulation processes of the reactive catalytic columns with intensification purpose.

6. Conclusions

This work analyzes the problem of mass and heat transport with surface chemical reaction in the catalytic porous medium in the reactive packing catalytic with an upscaling approach. A first-order reaction rate with an Arrhenius-type was considered. The governing equations at the pore-scale were upscaled using the volume averaging theory to obtain average equations expressed in terms of effective mass and heat dispersion coefficients and reaction and volume heat distribution. The surface reaction term at the microscopic scale, which relates to the pore-scale mass and heat balance, was analyzed using a multivariate Taylor series expansion. The effective coefficients associated with the upscaled model were predicted based on the solution of the closure problems in 2D and 3D periodic representations of the catalytic packing. In the case of the mass upscaled model, the effective dispersion coefficients depend essentially on the microscopic reaction velocity, categorized by the Thiele modulus, and influenced by the velocity rate (*i.e.* the Péclet number). For the energy model, the effective coefficients are essentially influenced by the thermal properties of the phases and the velocity rate. The predictions of the thermal dispersion coefficients are consistent with previous work without chemical reactions. The volume heat distribution coefficient, associated with the surface source of reaction, is independent when the heat transfer is dominated by one of the phases and influenced by the velocity rate when there is competition between solid catalytic and fluid phase conductivity.

The particular dependence of the effective coefficients is dictated, in general, by the corresponding geometry of the unit cell. The predictive capabilities of the upscaled model are confirmed

through a reasonable comparison of the average concentration and temperature profiles of the upscaled equations and the microscopic simulations. Noticeable differences in some of the temperature profiles of the catalytic solid can be attributed to the effect of the chemical reaction on the surface temperatures. A likely correction involves analyzing the linearization method of the Arrhenius-type surface reaction and its particular dependence on temperature deviations at the interface in the treatment of surface heat sources.

It should be emphasized that the representative region of the microstructure of the catalytic porous media used in this work is limited to simple geometries. However, the unit cell concept considers more complicated models that include geometric features of the catalytic packing. On the other hand, the results of the simulations show the feasibility of using upscaled models, which incorporate the catalytic packing structure in the effective coefficients; within macroscopic simulation schemes without requiring complex pore-scale simulations of the dispersive reaction process proposed in the CFD methods. With this idea in mind, one could propose the use of upscaled models to analyze more complex process simulations involving the optimization and intensification of catalytic structures attached to macroscopic reactive separation intensification processes. It will require the development of models, under this upscaling approach, to represent the multicomponent and multiphase transport with reversible reactions considering the suitable condition for separation.

Declaration of Competing Interest

The authors declare that they have no known competing financial interests or personal relationships that could have appeared to influence the work reported in this paper.

Acknowledgments

This work was financially supported by CONACYT-México (Grant No. A1-S-40629). O.A.L.R. thanks the "Estancias Posdoctorales por México" program for postdoctoral scholarship (Grant No. 274032) and the Center for Applied Innovation in Competitive Technologiess, CIATEC A.C.. J.J.Q.R. and V.A.S.T. thank the "Cátedras-CONACYT" program (Project No. 965).

Appendix A. Closure problem for momentum transport

As is mentioned in the main text, the upscaling model for a single-phase flow is given by the Darcy-Forchheimer equation, Eq. (10), (Whitaker, 1996; Lasseux et al., 2011),

$$\langle \mathbf{v}_\beta \rangle = -\frac{\mathbf{H}_\beta}{\mu_\beta} \cdot (\nabla \langle p_\beta \rangle^\beta - \rho_\beta \mathbf{g}) \quad (\text{A.1})$$

where the apparent Permeability, \mathbf{H}_β^{-1} , related both the intrinsic Permeability, \mathbf{K}_β , and the Forchheimer correction, \mathbf{F}_β , as

$$\mathbf{H}_\beta^{-1} = \mathbf{K}_\beta^{-1} \cdot (\mathbf{I} + \mathbf{F}_\beta) \quad (\text{A.2})$$

The upscaling model in the Eq. A.1, inherently involves the following length-scale and steady flow constraints: $\ell_\beta \ll r_0 \ll L$ and $\frac{\mu_\beta v_\beta^*}{\rho_\beta \ell_\beta^2} \ll 1$ or $\rho_\beta \frac{\langle v_\beta \rangle^\beta \ell_\beta}{\mu_\beta} (\ell_\beta/L) \ll 1$, which is according to the constraints used in this work. The tensor \mathbf{H}_β can be determined from the solution over the unit cell of the periodic structure (period $l_k, k = 1, 2, 3$) of the following closure problem

$$\begin{aligned} \text{Problem : } i = 0; \quad \text{Source : } 0 = \nabla \langle v_\beta \rangle^\beta; \\ \nabla \cdot \mathbf{E}_\beta = 0, \text{ in } \mathcal{V}_\beta \end{aligned} \quad (\text{A.3a})$$

$$\left(\frac{\rho_\beta v_\beta}{\mu_\beta}\right) \cdot \nabla \mathbf{E}_\beta = -\nabla e_\beta + \nabla^2 \mathbf{E}_\beta + \mathbf{I} \ln \psi_\beta \quad (\text{A.3b})$$

$$\mathbf{E}_\beta = \mathbf{0}, \text{ at } \mathcal{A}_{\beta\sigma} \quad (\text{A.3c})$$

$$\mathbf{E}_\beta(\mathbf{r} + \mathbf{l}_k) = \mathbf{E}_\beta(\mathbf{r}), k = 1, 2, 3 \quad (\text{A.3d})$$

$$e_\beta(\mathbf{r} + \mathbf{l}_k) = e_\beta(\mathbf{r}), k = 1, 2, 3 \quad (\text{A.3e})$$

$$\langle \mathbf{e}_\beta \rangle^\beta = \mathbf{0} \quad (\text{A.3f})$$

$$\langle \mathbf{E}_\beta \rangle = \mathbf{H}_\beta \quad (\text{A.3g})$$

As is given in (Lasseux et al., 2011), for low Reynolds number, $Re \leq 10$, where is defined as $Re = \rho_\beta v_{ref} \ell_c / \mu_\beta$ and v_{ref} is a reference velocity related with $\nabla \langle p_\beta \rangle^\beta$, the term $\left(\frac{\rho_\beta v_\beta}{\mu_\beta}\right) \cdot \nabla \mathbf{E}_\beta$ in the Eq. A.3b can be neglected. The latter results to $\mathbf{H}_\beta = \mathbf{K}_\beta$. In this work, the closure problem is solved in the representation geometry of the catalyst layer that consists of in-line cylinders (2D) and spheres (3D) unit cells (sketched in Fig. ??). The computation of the closure problem is performed using commercial finite element solvers involving adaptive mesh refinements to ensure that the results are independent of the number of elements. From the closure problem solution field, the values of the longitudinal intrinsic permeability $K_{\beta,xx}$ is computed using the expression in Eq. (A.3g), the predictions are presented in Fig. A.1 for the porosity variations. The results can fit successfully to the expressions given in the Eq. (11b) ($R^2 = 0.999$).

Appendix B. Closure problems

In this section, we present the details concerning in development of the formal solution to the closure problem associated with the upscaling model that describes the mass and heat transfer involving the reaction in the catalytic solid surface.

B.1. Mass transport

In the case of mass balance, from the main work, we summarize the boundary-value problem for the concentration deviation $\tilde{c}_{A\beta}$ indicating explicitly the source terms, as

$$\begin{aligned} & \tilde{v}_\beta \cdot \nabla \langle c_{A\beta} \rangle^\beta \text{Convectivesource} + v_\beta \cdot \nabla \tilde{c}_{A\beta} = \nabla \cdot (\nabla \mathcal{D}_\beta \tilde{c}_{A\beta}) \\ & + k_{(T_\sigma)^\sigma} \omega_1 a_v \langle c_{A\beta} \rangle^\beta \varepsilon_\beta^{-1} \text{Volumereactivesource} + \frac{k_{(T_\sigma)^\sigma} \omega_2}{V_\beta} \int_{A_{\beta\sigma}} \tilde{c}_{A\beta} dA \text{ in } V_\beta \end{aligned} \quad (\text{B.1a})$$

$$-n_{\beta\sigma} \cdot \mathcal{D}_\beta \nabla \tilde{c}_{A\beta} = -n_{\beta\sigma} \cdot \underbrace{\mathcal{D}_\beta \nabla \langle c_{A\beta} \rangle^\beta}_{\text{Diffusivesource}} \quad (\text{B.1b})$$

$$+ k_{(T_\sigma)^\sigma} \omega_1 \langle c_{A\beta} \rangle^\beta \text{Surfaceactivesource}$$

$$+ k_{(T_\sigma)^\sigma} \omega_2 \tilde{c}_{A\beta} \text{ at } A_{\beta\sigma}$$

$$\text{Periodicity: } \tilde{c}_{A\beta}(\mathbf{r}) = \tilde{c}_{A\beta}(\mathbf{r} + \mathbf{l}_i), i = 1, 2, 3 \quad (\text{B.1c})$$

$$\text{Restriction: } \langle \tilde{c}_{A\beta} \rangle^\beta = 0 \quad (\text{B.1d})$$

The fluid velocity field, v_β and its deviations, in the Eq. (B.1a), can be determined as a first instance from the solution of the Navier-Stokes equation. An alternative formulation suggests that the velocity field can be replaced by the average velocity defined in Eq. (A.1). Therefore, in the framework of volume averaging, it is possible to rewrite the closure problem only in terms of only closure variables (Valdés-Parada et al., 2017). The concentration deviations result from the convective effects, diffusive and reactive (superficial and volume) sources. In this case, the reactive source is associated with the reaction rate defined as $\langle T_\sigma \rangle^\sigma$. The formal solution to the boundary problem can be carried out based on the linear nature of the closure problem; the solution can be proposed in terms of the sources using superposition. However, as is indicated in previous works, the solution can be formulated formally using integrals equations based on Green's transformation functions (Valdés-Parada et al., 2011; Wood and Valdés-Parada, 2013). The result is expressed as

$$\tilde{c}_{A\beta} = f_\beta \cdot \nabla \langle c_{A\beta} \rangle^\beta + g_\beta \langle c_{A\beta} \rangle^\beta \quad (\text{B.2})$$

where f_β and g_β are being the so-called closure variables. The solution of the closure variable is obtained by solving the corresponding boundary-value problems, which result from subsisting Eq. (B.2) into Eqs. B.1a, B.1c, B.1d. The respective closure boundary-value problems are summarized as follows,

$$\text{Problem: } i = 1, 2 \quad \text{Source: } 1 = \nabla \langle c_{A\beta} \rangle^\beta; 2 = \langle c_{A\beta} \rangle^\beta \quad (\text{B.3a})$$

$$v_\beta \cdot \nabla \phi_i = \nabla \cdot (\mathcal{D}_\beta \nabla \phi_i) - f_i \quad (\text{B.3b})$$

$$-n_{\beta\sigma} \cdot \mathcal{D}_\beta \nabla \phi_i = g_i^I + g_i^II \text{ at } \mathcal{A}_{\beta\sigma} \quad (\text{B.3c})$$

$$\text{Periodicity: } \phi_i(\mathbf{r}) = \phi_i(\mathbf{r} + \mathbf{l}_k), k = 1, 2, 3 \quad (\text{B.3d})$$

$$\text{Restriction: } \langle \phi_i \rangle^\beta = 0 \quad (\text{B.3d})$$

where ϕ_i ($i = 1, 2$) represents the vectorial and scalar closure fields defined as $\phi_1 = f_\beta$ and $\phi_2 = g_\beta$. In addition, we introduce the volume and surface sources and integral terms using the expressions,

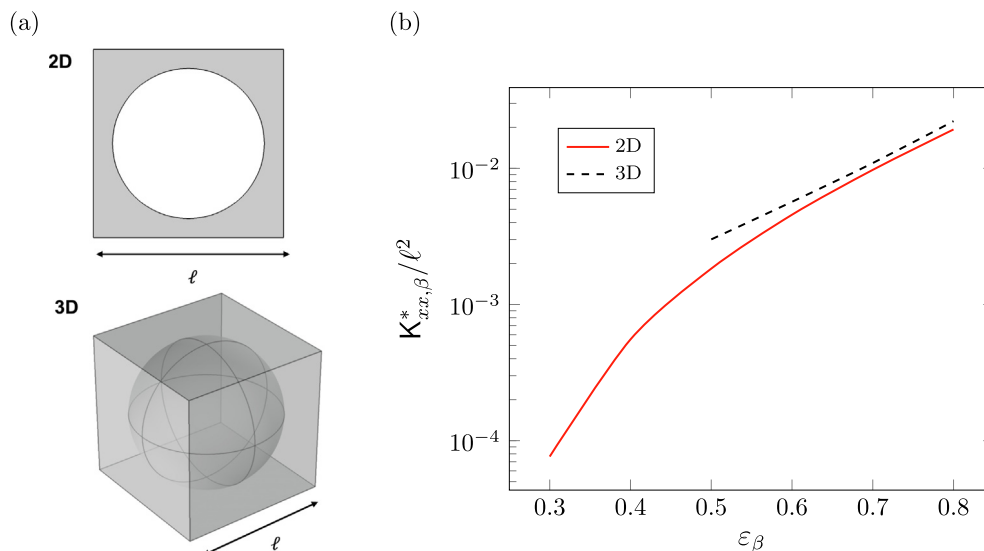


Fig. A.1. (a) Unit cell representative of a catalytic bed (b) Intrinsic permeability as function of porosity for 2D and 3D unit cells.

$$f_i = \delta_{i1} \tilde{v} - \delta_{i2} k_{(T_\sigma)^\sigma} \omega_1 a_v \varepsilon_\beta^{-1} - \frac{k_{(T_\sigma)^\sigma} \omega_2}{V_\beta} \int_{\mathcal{A}_{\beta\sigma}} \phi_i dA \quad (\text{B.4a})$$

$$g_i^I = \delta_{i1} n_{\beta\sigma} \mathcal{D}_\beta, \quad (\text{B.4b})$$

$$g_i^{II} = \delta_{i1} k_{(T_\sigma)^\sigma} \omega_2 \phi_i + \delta_{i2} k_{(T_\sigma)^\sigma} (\omega_1 + \omega_2 \phi_i) \quad (\text{B.4c})$$

If we carry out an order magnitude analysis, the fields of both the closure variables depend on the reaction rate coefficient $k_{(T_\sigma)^\sigma}$ Eqs. (B.3a)–(B.3d), we have

$$f_\beta = O\left(\frac{\ell_\beta}{1 + \varphi^2}\right), g_\beta = O\left(\frac{\varphi^2}{1 + \varphi^2}\right) \quad (\text{B.5})$$

where φ represents Thiele's modulus, defined as $\varphi = \sqrt{k \frac{\ell_\beta^2}{\mathcal{D}_\beta}}$.

Here we assume ω_1 and $\omega_2 = O(1)$. We can consider that the closure problems associated with mass transport are independent of the local quantities and constant on the microscopic scale. The algorithm to compute the effective coefficient consists at first of solving the Navier–Stokes, Eqs. (1a)–(1c), imposing a gradient pressure in the longitudinal direction in the unit cell of the catalytic bed of circle (2D) and sphere (3D) obstacles, A.1 (a). The determination of the velocity field is used as input for solving the closure problem using the finite element solver; examples of the closure variable fields are shown in Fig. B.1. Finally, the results of variable closure fields are substituted in Eqs. (37) and (38) to compute the effective coefficients presented in the main text.

B.2. Heat transport

Following the closure problem for the heat transport macroscopic model, the governing equation and the boundary conditions for the temperature deviations are expressed as

$$\begin{aligned} & (\rho c_p)_\beta v_\beta \cdot \nabla \tilde{T}_\beta + \underbrace{(\rho c_p)_\beta \tilde{v}_\beta \cdot \nabla \langle T_\beta \rangle^\beta}_{\text{convective source}} \\ & = \nabla \cdot \left(k_\beta \nabla \tilde{T}_\beta \right) - \frac{\varepsilon_\beta^{-1} k_\beta}{V} \int_{\mathcal{A}_{\beta\sigma}} n_{\beta\sigma} \cdot \nabla \tilde{T}_\beta dA, \text{en} \mathcal{V}_\beta \end{aligned} \quad (\text{B.6a})$$

$$0 = \nabla \cdot \left(k_\sigma \nabla \tilde{T}_\sigma \right) - \frac{\varepsilon_\sigma^{-1} k_\sigma}{V} \int_{\mathcal{A}_{\beta\sigma}} n_{\sigma\beta} \cdot \nabla \tilde{T}_\sigma dA, \text{en} \mathcal{V}_\sigma \quad (\text{B.6b})$$

$$\tilde{T}_\beta = \tilde{T}_\sigma + \underbrace{\left(\langle T_\sigma \rangle^\sigma - \langle T_\beta \rangle^\beta \right)}_{\text{Interfacial source}}, \text{en} \mathcal{A}_{\beta\sigma} \quad (\text{B.6c})$$

$$\begin{aligned} & -n_{\beta\sigma} \cdot k_\beta \nabla \tilde{T}_\beta = -n_{\beta\sigma} \cdot k_\sigma \nabla \tilde{T}_\sigma \\ & + \underbrace{n_{\beta\sigma} \cdot k_\beta \nabla \langle T_\beta \rangle^\beta - n_{\beta\sigma} \cdot k_\sigma \nabla \langle T_\sigma \rangle^\sigma}_{\text{Conductive source}} \end{aligned} \quad (\text{B.6d})$$

$$+ \underbrace{S_{rxn} H = q_{rxn}}_{\text{Reactive source}} \text{en} \mathcal{A}_{\beta\sigma} \quad (\text{B.6e})$$

$$\text{Periodicity : } \tilde{T}_\alpha(r) = \tilde{T}_\alpha(r + l); \alpha = \beta, \sigma; i = 1, 2, 3 \quad (\text{B.6f})$$

$$\text{Restriction : } \langle \tilde{T}_\alpha \rangle^\alpha = 0; \alpha = \beta, \sigma \quad (\text{B.6g})$$

The periodicity conditions in this boundary-value problem, Eq. (B.6f), replace external boundary conditions of the system. We are not interested in solving this equations system in the macroscopic system. A representative periodic unit cell of the microscopic of the catalytic system provides an accurate representation of the external boundary conditions to solve the closure problem. The restriction of the intrinsic average of the deviations is zero, Ec. B.6g (and Ec. B.1d), for mass closure problem), is consequence from the separations of length-scales separation assumption (Eq. 6). According to (Wood and Valdés-Parada, 2013), these results arise from the upscale postulates. The formal solution of the boundary-value problem for the

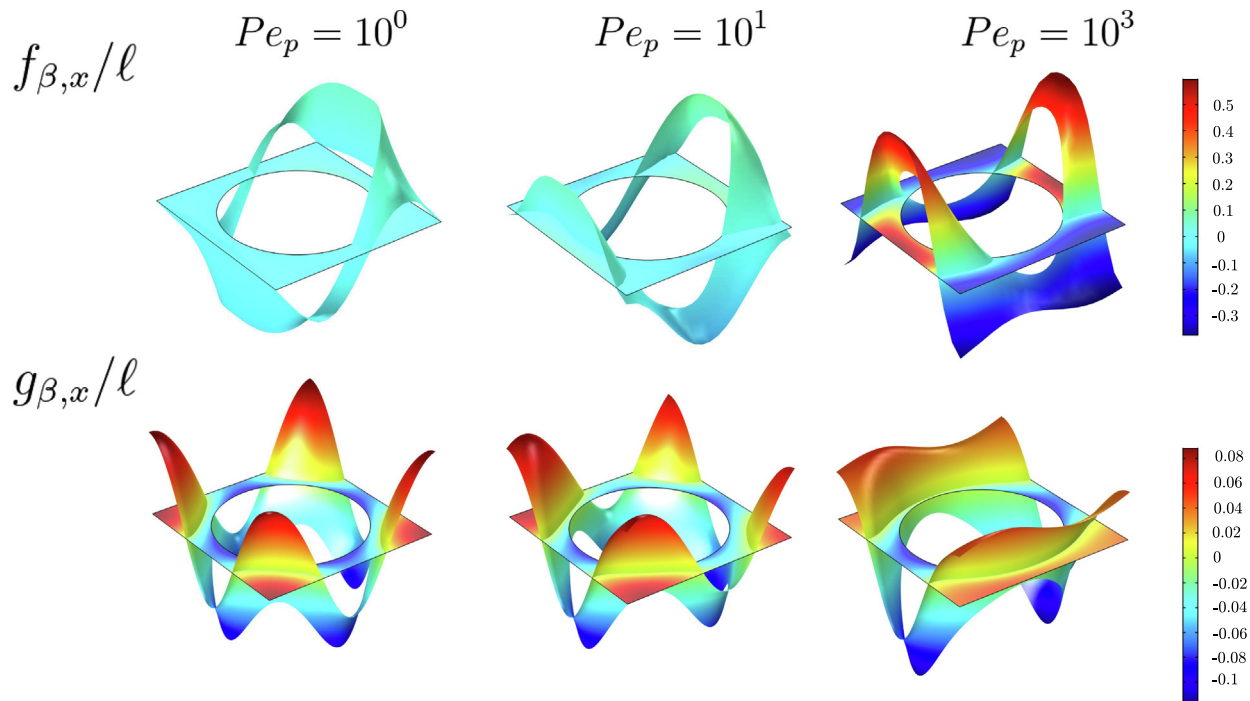


Fig. B.1. Fields of closure variables for $f_{\beta x}$ and $g_{\beta x}$ in the direction of the fluid flow component for $\varepsilon_\beta = 0.5$ and $\varphi = 1$.

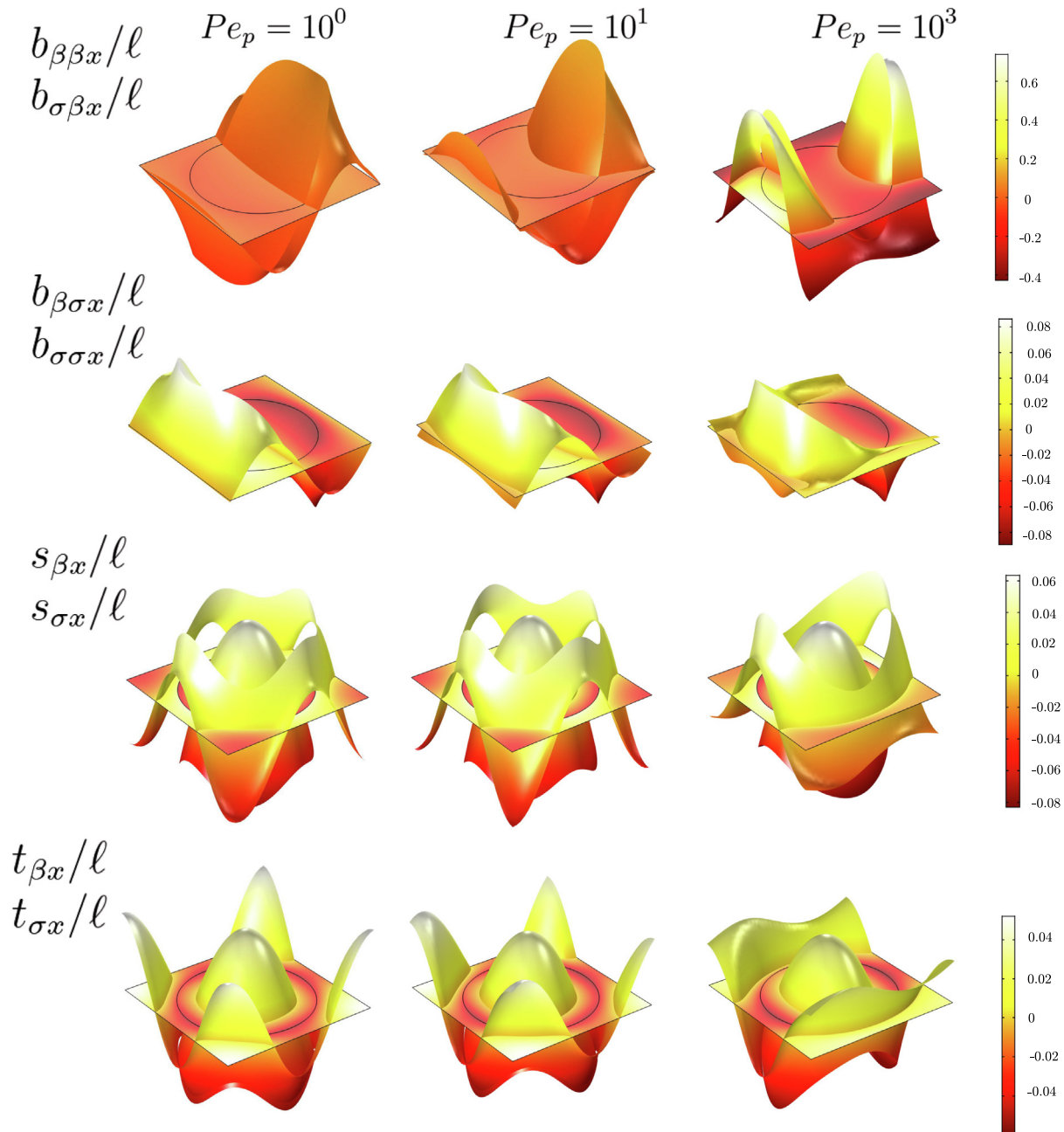


Fig. B.2. Fields of closure variables for $b_{j\sigma x}, b_{\sigma j x}, s_j, t_j$; $j = \beta, \sigma$ for $\varepsilon_\beta = 0.5$ and $\kappa = 1$.

temperature deviations can be derived using integral Green’s transformations. However, as is indicated in the previous closure problem, the linear nature of the boundary value, it is plausible to propose a solution in terms of the indicating sources as follows,

$$\tilde{T}_\beta = b_{\beta\beta} \cdot \nabla \langle T_\beta \rangle^\beta + b_{\beta\sigma} \cdot \nabla \langle T_\sigma \rangle^\sigma - s_\beta (\langle T_\beta \rangle^\beta - \langle T_\sigma \rangle^\sigma) + r_\beta (q_{rxn}) \quad (B.7a)$$

$$\tilde{T}_\sigma = b_{\sigma\beta} \cdot \nabla \langle T_\beta \rangle^\beta + b_{\sigma\sigma} \cdot \nabla \langle T_\sigma \rangle^\sigma + s_\beta (\langle T_\sigma \rangle^\sigma - \langle T_\beta \rangle^\beta) + r_\sigma (q_{rxn}) \quad (B.7b)$$

where $b_{\beta\beta}, b_{\beta\sigma}, b_{\sigma\sigma}, b_{\sigma\beta}, s_\beta, s_\sigma, r_\beta$ and r_σ are the calling the closure variables, in the literature they have represented in terms of integrals of associated Green’s functions (Wood and Valdés-Parada, 2013). The expressions in the Eq. (B.7), is consistent with previous works for passive heat transfer in porous media (Quintard et al.,

1997; Dispersion in heterogeneous porous media: One-equation non-equilibrium model, 2001; Aguilar-Madera et al., 2011). In this case, the active heat transfer in porous media, given the influence superficial chemical reaction source, is associated with the closure variables r_β and r_σ , which signs how this source is distributed in the average temperature of the solid and fluid phases. This aspect is appreciated in the last term in the macroscopic heat transfer model, Eqs. (41) and (42), where the effective coefficients are correlated with the average reaction term. The solution field of the closure variables is determined by solving the corresponding boundary-value problems obtained by substituting Eqs. (B.7) into Eqs. (B.6). These problems, indicating the associated source, can be summarized as follows

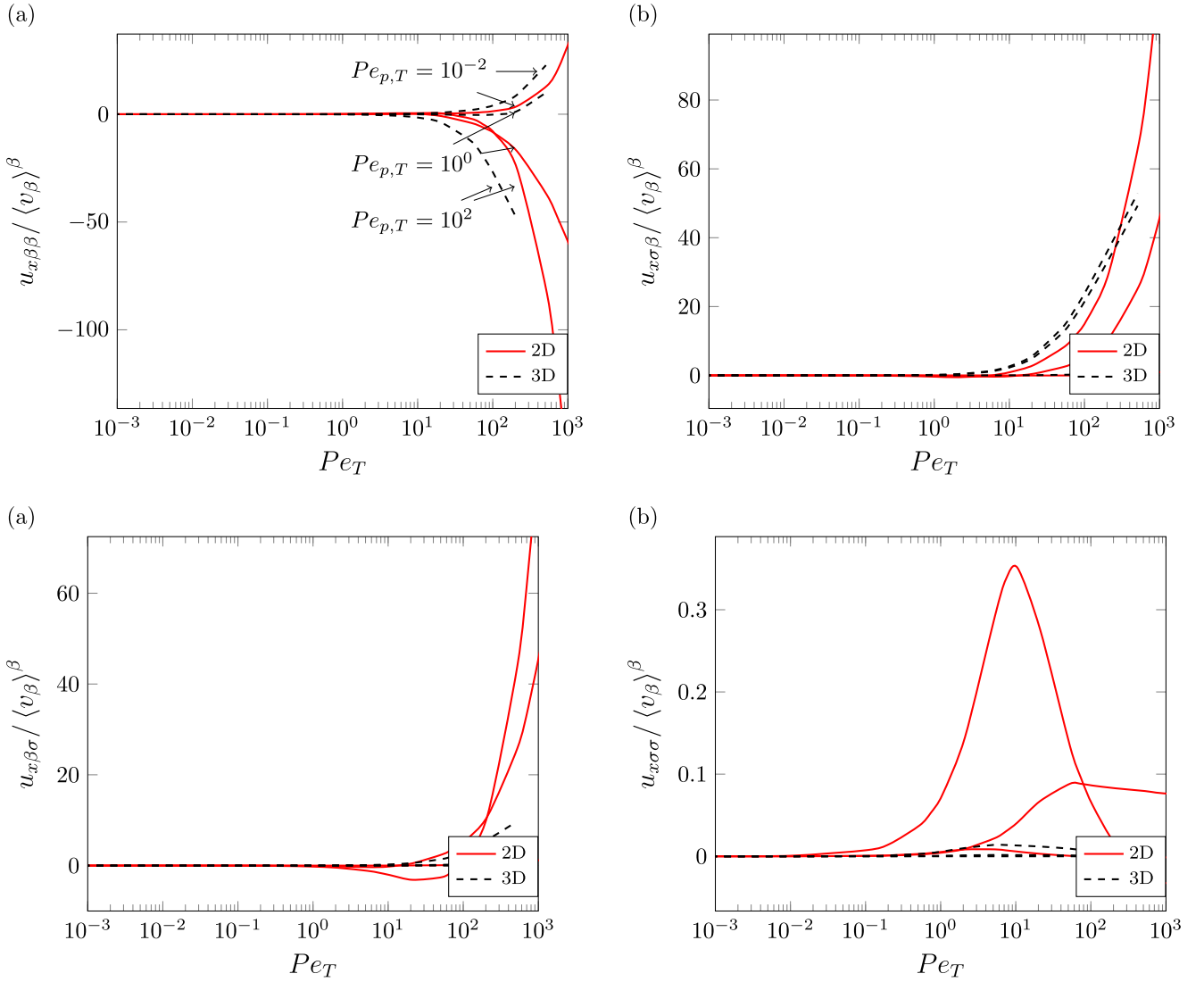


Fig. B.3. (a) Convective coefficient $i \cdot u_{\beta\beta}$, (b) Convective coefficient $i \cdot u_{\sigma\beta}$, (c) Convective coefficient $i \cdot u_{\beta\sigma}$, (d) $i \cdot u_{\sigma\sigma}$, $\kappa = 10^0$ and $\varepsilon_\beta = 0.5$.

Problem : $i = 3, 4, 5, 6$ Source : $3 = \nabla \langle T_\beta \rangle^\beta$;

$$4 = \nabla \langle T_\sigma \rangle^\sigma; 5 = \langle T_\beta \rangle^\beta - \langle T_\sigma \rangle^\sigma; 6 = q_{rxn} \quad (\text{B.8a})$$

$(\rho c_p)_\beta v_\beta \cdot \nabla \phi_{\beta i} = k_\beta \nabla^2 \phi_{\beta i} - f_{\beta i}$, in the β - phase

$$0 = k_\sigma \nabla^2 \phi_{\sigma i} - f_{\sigma i}, \text{ in the } \sigma \text{ - phase} \quad (\text{B.8b})$$

$$\phi_{\beta i} = \phi_{\sigma i} + \mathbf{g}_i^I, \text{ at } \mathcal{A}_{\beta\sigma} \quad (\text{B.8c})$$

$$\mathbf{n}_{\beta\sigma} \cdot k_\beta \nabla \phi_\beta = \mathbf{n}_{\beta\sigma} \cdot k_\sigma \nabla \phi_\sigma + \mathbf{g}_i^II, \text{ at } \mathcal{A}_{\beta\sigma} \quad (\text{B.8d})$$

$$\text{Periodicity : } \phi_{\beta i}(\mathbf{r}) = \phi_{\beta i}(\mathbf{r} + l_k), \phi_{\sigma i}(\mathbf{r}) = \phi_{\sigma i}(\mathbf{r} + l_k); k = 1, 2, 3 \quad (\text{B.8e})$$

$$\text{Restriction : } \langle \phi_{\beta i} \rangle^\beta = \langle \phi_{\sigma i} \rangle^\sigma = 0; \quad (\text{B.8f})$$

where ϕ_{ij} ($j = \beta, \sigma; i = 3, 4, 5, 6$) represent the vectorial and scalar fields according to

$$\phi_{j3} = b_{j\beta}; \phi_{j4} = b_{j\sigma}; \phi_{j5} = S_j; \phi_{j6} = r_j; j = \beta, \sigma \quad (\text{B.9})$$

where f_{mi} in the Eqs. (B.8a) and (B.8b), is expressing as

$$f_{mi} = \delta_{i1} \delta_{m\beta} (\rho c_p)_m \tilde{v}_\beta + \frac{\varepsilon_m^{-1} k_m (-1)^{\delta_{m\sigma}}}{V} \int_{\mathcal{A}_{\beta\sigma}} \mathbf{n}_{\beta\sigma} \cdot \nabla \phi_{mi} dA, m = \beta, \sigma, i = 1, 2, 3 \quad (\text{B.10a})$$

$$\mathbf{g}_i^I = \delta_{i3} \mathbf{g}_i^I, \mathbf{g}_i^II = \mathbf{n}_{\beta\sigma} (-\delta_{i1} + \delta_{2i} k_\sigma) + \delta_{4i}, i = 1, 2, 3 \quad (\text{B.10b})$$

Similar to previous closure problems related to momentum and mass upscaling transport equations, Closure Problems 3,4,5 and 6 were solved in 2D and 3D unit cells with the simple geometrical as sketched in Fig. A.1. It emphasizes that the geometry can be more complex and include structural details of the catalysts. The expressions of the effective coefficients, introduced in Eqs. (41) and (42), can be summarized respectively with the closure variables as follows

$$\mathbf{K}_{ij}^{\delta_{i\beta}} = k_i \left[\varepsilon_i \delta_{ij} \mathbf{I} + \frac{(-1)^{\delta_{i\sigma}}}{V} \int_{\mathcal{A}_{\beta\sigma}} \mathbf{n}_{\beta\sigma} b_{ij} dA - \delta_{i\beta} (\rho c_p)_i \langle \tilde{v}_i b_{ij} \rangle \right] \quad (\text{B.11a})$$

$$\mathbf{u}_{ij}^{\delta_{i\beta}} = \frac{\alpha_i}{\mathcal{V}} \left[(-1)^{\delta_{i\sigma}} \int_{\mathcal{A}_{\beta\sigma}} \mathbf{n}_{\beta\sigma} \cdot \nabla b_{ij} dA + (-1)^{\delta_{ij}} \int_{\mathcal{A}_{\beta\sigma}} \mathbf{n}_{\beta\sigma} s_i dA - \delta_{i\beta} (-1)^{\delta_{i\beta}} \langle \tilde{v}_i s_i \rangle \right] \quad (\text{B.11b})$$

$$\mathbf{a}_v h = \frac{k_i}{\mathcal{V}} \int_{\mathcal{A}_{\beta\sigma}} \mathbf{n}_{\beta\sigma} \cdot \nabla s_i dA \quad (\text{B.11c})$$

$$\zeta_i = \frac{k_i}{\mathcal{A}_{\beta\sigma}} \int_{\mathcal{A}_{\beta\sigma}} \mathbf{n}_{\beta\sigma} \cdot \nabla r_i dA, \quad \zeta_\beta + \zeta_\sigma = 1 \quad (\text{B.11d})$$

in these equations $i = \beta, r; j = \beta, \sigma$, while α_i represents the thermal diffusivity of the i - phase ($i = \beta, \sigma$). (See Figs. B.2 and B.3)

References

- Aguilar-Madera, C.G., Valdés-Parada, F.J., Goyeau, B., Alberto Ochoa-Tapia, J., 2011. One-domain approach for heat transfer between a porous medium and a fluid. *Int. J. Heat Mass Transf.* 54 (9), pp. 2089–2099. doi: 10.1016/j.ijheatmasstransfer.2010.12.020. URL: <https://www.sciencedirect.com/science/article/pii/S001793101000712X>.
- Amini, Y., Nasr Esfahany, M., 2019. Cfd simulation of the structured packings: A review. *Sep. Sci. Technol. (Philadelphija)* 54 (15), pp. 2536 – 2554, cited by: 36. doi:10.1080/01496395.2018.1549078. URL: <https://www.scopus.com/inward/record.uri?eid=2-s2.0-85065772454&doi=10.1080%2F01496395.2018.1549078&partnerID=40&md5=409e8242b59ecc9f6a8e6ed596d8ccda>.
- Bear, J., Cheng, A.H.-D., 2018. *Modeling groundwater flow and contaminant transport*, Vol. 23. Springer Science & Business Media.
- Chemical Reactor Analysis and Design, Wiley, 2010.
- Cheremisinoff, N.P., 1989. Handbook of heat and mass transfer volume 3: Catalysis, kinetics, and reactor engineering. URL: <https://www.osti.gov/biblio/7090242>.
- de los Santos-Sánchez, R., Valdés-Parada, F.J., Chirino, Y.I., 2016. Upscaling diffusion and reaction processes in multicellular systems considering different cell populations. *Chem. Eng. Sci.* 142, pp. 144–164. doi: <https://doi.org/10.1016/j.ces.2015.11.031>. URL: <https://www.sciencedirect.com/science/article/pii/S009250915007551>
- Dispersion in heterogeneous porous media: One-equation non-equilibrium model. *Transp. Porous Media* 44 (1), pp. 181–203. doi:10.1023/A:1010746011296. URL: <https://doi.org/10.1023/A:1010746011296>
- Egorov, Y., Menter, F., Klöcker, M., Kenig, E., 2005. On the combination of cfd and rate-based modelling in the simulation of reactive separation processes. *Chem. Eng. Process.: Process Intens.* 44 (6), pp. 631–644, intelligent Column Internals for Reactive Separations. doi: 10.1016/j.cep.2003.10.011. URL: <https://www.sciencedirect.com/science/article/pii/S0255270104001953>.
- Goortani, B.M., Gaurav, A., Deshpande, A., Ng, F.T.T., Rempel, G.L., 2015. Production of isooctane from isobutene: Energy integration and carbon dioxide abatement via catalytic distillation. *Industr. Eng. Chem. Res.* 54 (14), 3570–3581. <https://doi.org/10.1021/ie5032056>. URL: <https://doi.org/10.1021/ie5032056>.
- Gray, W.G., 1975. A derivation of the equations for multi-phase transport. *Chem. Eng. Sci.* 30 (2), 229–233. [https://doi.org/10.1016/0009-2509\(75\)80010-8](https://doi.org/10.1016/0009-2509(75)80010-8). URL: <https://www.sciencedirect.com/science/article/pii/0009250975800108>.
- Gray, W.G., Miller, C.T., 2013. A generalization of averaging theorems for porous medium analysis. *Adv. Water Resour.* 62, pp. 227–237, a tribute to Stephen Whitaker. doi: 10.1016/j.advwatres.2013.06.006. URL: <https://www.sciencedirect.com/science/article/pii/S0309170813001073>.
- Gray, W.G., Miller, C.T., 2014. *Introduction to the thermodynamically constrained averaging theory for porous medium systems*. Springer.
- Guo, J., Quintard, M., Laouafa, F., 2015. Dispersion in porous media with heterogeneous nonlinear reactions. *Transp. Porous Media* 109 (3), 541–570. <https://doi.org/10.1007/s11242-015-0535-4>.
- Haase, S., Tolvanen, P., Russo, V., 2022. Process intensification in chemical reaction engineering. *Processes* 10 (1). <https://doi.org/10.3390/pr10010099>. URL: <https://www.mdpi.com/2227-9717/10/1/99>.
- Harmsen, G.J., 2007. Reactive distillation: The front-runner of industrial process intensification: A full review of commercial applications, research, scale-up, design and operation, *Chemical Engineering and Processing: Process Intensification* 46 (9) (2007) 774–780, selected Papers from the European Process Intensification Conference (EPIC), Copenhagen, Denmark, September 19–20, 2007. doi: 10.1016/j.cep.2007.06.005. URL: <https://www.sciencedirect.com/science/article/pii/S0255270107002085>.
- Heße, F., Radu, F., Thullner, M., Attinger, S., 2009. Upscaling of the advection-diffusion-reaction equation with monod reaction. *Adv. Water Resour.* 32 (8), 1336–1351. <https://doi.org/10.1016/j.advwatres.2009.05.009>. URL: <https://www.sciencedirect.com/science/article/pii/S0309170809000918>.
- Hong, A., Zhang, Z., Li, X., Gao, X., 2021. A generalized cfd model for evaluating catalytic separation process in structured porous materials. *Chin. J. Chem. Eng.* <https://doi.org/10.1016/j.cjche.2021.12.004>. URL: <https://www.sciencedirect.com/science/article/pii/S1004954121006042>.
- Howes, F.A., Whitaker, S., 1985. The spatial averaging theorem revisited. *Chem. Eng. Sci.* 40 (8), 1387–1392. [https://doi.org/10.1016/0009-2509\(85\)80078-6](https://doi.org/10.1016/0009-2509(85)80078-6). URL: <https://www.sciencedirect.com/science/article/pii/0009250985800786>.
- Lasseux, D., Abbasian Arani, A.A., Ahmadi, A., 2011. On the stationary macroscopic inertial effects for one phase flow in ordered and disordered porous media. *Phys. Fluids* 23 (7), 073103. arXiv: <https://doi.org/10.1063/1.3615514>. doi:10.1063/1.3615514. URL: doi:10.1063/1.3615514.
- Lasseux, D., Valdés Parada, F.J., Porter, M.L., 2016. An improved macroscale model for gas slip flow in porous media. *J. Fluid Mech.* 805, 118–146. <https://doi.org/10.1017/jfm.2016.562>.
- Lei, Z., Yang, Y., Li, Q., Chen, B., 2009. Catalytic distillation for the synthesis of tert-butyl alcohol with structured catalytic packing. *Catal. Today* 147, pp. S352–S356, 3rd International Conference on Structured Catalysts and Reactors, ICOSCAR-3, Ischia, Italy, 27–30 September 2009. doi: 10.1016/j.cattod.2009.07.040. URL: <https://www.sciencedirect.com/science/article/pii/S0920586109004040>.
- Lugo-Méndez, H.D., Valdés-Parada, F.J., Porter, M.L., Wood, B.D., Ochoa-Tapia, J.A., 2015. Upscaling diffusion and nonlinear reactive mass transport in homogeneous porous media. *Transp. Porous Media* 107 (3), 683–716. <https://doi.org/10.1007/s11242-015-0462-4>. URL: <https://doi.org/10.1007/s11242-015-0462-4>.
- Macfarlan, L.H., Phan, M.T., Eldridge, R.B., 2022. Methodologies for predicting the mass transfer performance of structured packings with computational fluid dynamics: A review. *Chem. Eng. Process. - Process Intensif.* 172, 108798. <https://doi.org/10.1016/j.cep.2022.108798>. URL: <https://www.sciencedirect.com/science/article/pii/S0255270122000216>.
- Mauri, R., 1991. Dispersion, convection, and reaction in porous media. *Phys. Fluids A* 3, 743–756. <https://doi.org/10.1063/1.858007>. URL: <http://aip.scitation.org/doi/10.1063/1.858007>.
- M. Mazarei Sotoodeh, M. Zivdar, R. Rahimi, Cfd modeling of multiphase flow in reactive distillation column, *Chemical Engineering and Processing - Process Intensification* 129 (2018) 1–9. doi: <https://doi.org/10.1016/j.cep.2018.04.034>. URL: <https://www.sciencedirect.com/science/article/pii/S025527011830165X>
- Ochoa-Tapia, J., Whitaker, S., 1997. Heat transfer at the boundary between a porous medium and a homogeneous fluid. *Int. J. Heat Mass Transf.* 40 (11), 2691–2707. [https://doi.org/10.1016/S0017-9310\(96\)00250-5](https://doi.org/10.1016/S0017-9310(96)00250-5). URL: <https://www.sciencedirect.com/science/article/pii/S0017931096002505>.
- Porta, G.M., Riva, M., Guadagnini, A., 2012. Upscaling solute transport in porous media in the presence of an irreversible bimolecular reaction. *Adv. Water Resour.* 35, 151–162. <https://doi.org/10.1016/j.advwatres.2011.09.004>. URL: <https://www.sciencedirect.com/science/article/pii/S0309170811001710>.
- Porter, M.L., Valdés-Parada, F.J., Wood, B.D., 2010. Comparison of theory and experiments for dispersion in homogeneous porous media. *Adv. Water Resour.* 33 (9), 1043–1052. <https://doi.org/10.1016/j.advwatres.2010.06.007>. URL: <https://www.sciencedirect.com/science/article/pii/S0309170810001193>.
- Qiu, T., Wang, Q., Yang, C., 2017. Upscaling multicomponent transport in porous media with a linear reversible heterogeneous reaction. *Chem. Eng. Sci.* 171, 100–116.
- Quintard, M., Whitaker, S., 1993. One- and two-equation models for transient diffusion processes in two-phase systems, Vol. 23 of *Advances in Heat Transfer*, Elsevier, 1993, pp. 369–464. doi: 10.1016/S0065-2717(08)70009-1. URL: <https://www.sciencedirect.com/science/article/pii/S0065271708700091>.
- Quintard, M., Kaviany, M., Whitaker, S., 1997. Two-medium treatment of heat transfer in porous media: numerical results for effective properties. *Adv. Water Resour.* 20 (2), pp. 77–94, advances in Heat Transfer in Porous Media. doi: 10.1016/S0309-1708(96)00024-3. URL: <https://www.sciencedirect.com/science/article/pii/S0309170896000243>.
- Quintard, M., Whitaker, S., 2000. Theoretical analysis of transport in porous media, *Handbook of Porous Media*. In: Hadim, H., Vafai, K. (Eds), *Handbook of Heat Transfer in Porous Media* (2000) 1–52. URL: doi: 10.1201/b18614.
- Quintard, M., Bletzacker, L., Chenu, D., Whitaker, S., 2006. Nonlinear, multicomponent, mass transport in porous media. *Chem. Eng. Sci.* 61 (8), 2643–2669. <https://doi.org/10.1016/j.ces.2005.11.034>. URL: <https://www.sciencedirect.com/science/article/pii/S0009250905008924>.
- Ryan, D., 1983. Effective diffusivities in reactive porous media: a comparison between theory and experiments.
- Sanchez-Palencia, E., 1980. *Non-Homogeneous Media and Vibration Theory*, Lecture notes in physics, Springer, Berlin. doi:10.1007/3-540-10000-8. URL: <https://cds.cern.ch/record/1391389>
- Segovia-Hernández, J.G., Hernández, S., Bonilla Petriciolet, A., 2015. Reactive distillation: A review of optimal design using deterministic and stochastic techniques. *Chem. Eng. Process.* 97, 134–143. <https://doi.org/10.1016/j.cep.2015.09.004>. URL: <https://www.sciencedirect.com/science/article/pii/S0255270115300969>.
- Shapiro, M.A., Brenner, H., 1986. Taylor dispersion of chemically reactive species: Irreversible first-order reactions in bulk and on boundaries. *Chem. Eng. Sci.* 41, 1417–1433.
- Shapiro, M., Brenner, H., 1988. Dispersion of a chemically reactive solute in a spatially periodic model of a porous medium. *Chem. Eng. Sci.* 43 (3), 551–571. [https://doi.org/10.1016/0009-2509\(88\)87016-7](https://doi.org/10.1016/0009-2509(88)87016-7). URL: <https://www.sciencedirect.com/science/article/pii/0009250988870167>.
- Stankiewicz, A., 2003. Reactive separations for process intensification: an industrial perspective. *Chem. Eng. Process.* 42 (3), 137–144. [https://doi.org/10.1016/S0255-2701\(02\)00084-3](https://doi.org/10.1016/S0255-2701(02)00084-3). URL: <https://www.sciencedirect.com/science/article/pii/S0255270102000843>.
- Valdes-Parada, F., Alvarez-Ramirez, J., 2010. On the effective diffusivity under chemical reaction in porous media. *Chem. Eng. Sci.* 65 (13), 4100–4104. <https://doi.org/10.1016/j.ces.2010.03.040>. URL: <https://www.sciencedirect.com/science/article/pii/S009250910001880>.
- Valdés-Parada, F., Aguilar-Madera, C., Álvarez Ramirez, J., 2011. On diffusion, dispersion and reaction in porous media. *Chem. Eng. Sci.* 66 (10), pp. 2177–2190. doi: 10.1016/j.ces.2011.02.016. URL: <https://www.sciencedirect.com/science/article/pii/S0009250911001035>.
- Valdés-Parada, F.J., Lasseux, D., Whitaker, S., 2017. Diffusion and heterogeneous reaction in porous media: The macroscale model revisited. *Int. J. Chem. Reactor Eng.* 15 (6), 20170151. <https://doi.org/10.1515/ijcre-2017-0151>. URL: doi: 10.1515/ijcre-2017-0151.
- Valdés-Parada, F.J., Lasseux, D., Whitaker, S., 2020. Upscaling reactive transport under hydrodynamic slip conditions in homogeneous porous media. *Water Resour. Res.* 56 (1), e2019WR025954, e2019WR025954 10.1029/2019WR025954. arXiv: <https://agupubs.onlinelibrary.wiley.com/doi/pdf/10.1029/2019WR025954>, doi: 10.1029/2019WR025954. URL: <https://agupubs.onlinelibrary.wiley.com/doi/abs/10.1029/2019WR025954>.

- van Baten, J., Krishna, R., 2002. Gas and liquid phase mass transfer within katalapaks[®] structures studied using cfd simulations. *Chem. Eng. Sci.*, 57 (9), pp. 1531–1536, 2nd ISMR Nuremberg. doi: 10.1016/S0009-2509(02)00026-X. URL: <https://www.sciencedirect.com/science/article/pii/S000925090200026X>.
- Vynnycky, M., Birgersson, E., 2003. Analysis of a model for multicomponent mass transfer in the cathode of a polymer electrolyte fuel cell. *SIAM J. Appl. Math.* 63 (4), 1392–1423. URL: <http://www.jstor.org/stable/4095966>.
- Wang, Q., Yang, C., Wang, H., Qiu, T., 2017. Optimization of process-specific catalytic packing in catalytic distillation process: A multi-scale strategy. *Chem. Eng. Sci.* 174, 472–486. <https://doi.org/10.1016/j.ces.2017.09.040>. URL: <https://www.sciencedirect.com/science/article/pii/S0009250917305936>.
- Wang, Q., Liu, X., Wu, X., Yang, C., Qiu, T., 2020. A multi-scale approach to optimize vapor-liquid mass transfer layer in structured catalytic packing. *Chem. Eng. Sci.* 214, 115434. <https://doi.org/10.1016/j.ces.2019.115434>. URL: <https://www.sciencedirect.com/science/article/pii/S0009250919309248>.
- Whitaker, S., 1986. Local thermal equilibrium: An application to packed bed catalytic reactor design. *Chem. Eng. Sci.* 41 (8), 2029–2039. [https://doi.org/10.1016/0009-2509\(86\)87119-6](https://doi.org/10.1016/0009-2509(86)87119-6). URL: <https://www.sciencedirect.com/science/article/pii/0009250986871196>.
- Whitaker, S., 1987. Mass transport and reaction in catalyst pellets. *Transp. Porous Media* 2 (3), 269–299.
- Whitaker, S., 1991. Improved constraints for the principle of local thermal equilibrium. *Industr. Eng. Chem. Res.* 30 (5), 983–997. <https://doi.org/10.1021/ie00053a022>. URL: <https://doi.org/10.1021/ie00053a022>.
- Whitaker, S., 1996. The forchheimer equation: A theoretical development. *Transp. Porous Media* 25 (1), 27–61. <https://doi.org/10.1007/BF00141261>.
- Whitaker, S., 1999. *The method of volume averaging*. Kluwer Academic Publishers.
- Wood, B.D., 2009. The role of scaling laws in upscaling. *Adv. Water Resour.*, 32 (5), pp. 723–736, dispersion in Porous Media. doi: 10.1016/j.advwatres.2008.08.015. URL: <https://www.sciencedirect.com/science/article/pii/S0309170808001498>.
- Wood, B.D., Valdés-Parada, F.J., 2013. Volume averaging: Local and nonlocal closures using a green's function approach. *Adv. Water Resour.*, 51, PP. 139–167, 35th Year Anniversary Issue. doi: 10.1016/j.advwatres.2012.06.008. URL: <https://www.sciencedirect.com/science/article/pii/S0309170812001583>.
- Wood, B.D., Radakovich, K., Golfier, F., 2007. Effective reaction at a fluid–solid interface: Applications to biotransformation in porous media. *Adv. Water Resour.*, 30 (6), 1630–1647, biological processes in porous media: From the pore scale to the field. doi: 10.1016/j.advwatres.2006.05.032. URL: <https://www.sciencedirect.com/science/article/pii/S0309170806001400>.
- Xue, J., Li, Q., Qi, J., Wu, Q., Zhao, H., Zhang, L., 2021. Multi-scale study of wet pressure drop model for a novel structured wire gauze packing. *Chem. Eng. Sci.* 230, 116179. <https://doi.org/10.1016/j.ces.2020.116179>. URL: <https://www.sciencedirect.com/science/article/pii/S0009250920307119>.
- Yan, X., Li, N., 2017. Simulation of solute dispersion in particle packs by the volume averaging method. *Comput. Chem. Eng.* 98, 154–160. <https://doi.org/10.1016/j.compchemeng.2016.12.021>. URL: <https://www.sciencedirect.com/science/article/pii/S0098135416304264>.
- Yang, C., Thovert, J.-F., Debenest, G., 2015a. Upscaling of mass and thermal transports in porous media with heterogeneous combustion reactions. *Int. J. Heat Mass Transf.* 84, 862–875. <https://doi.org/10.1016/j.ijheatmasstransfer.2015.01.043>. URL: <https://www.sciencedirect.com/science/article/pii/S0017931015000502>.
- Yang, C., Quintard, M., Debenest, G., 2015b. Upscaling for adiabatic solid–fluid reactions in porous medium using a volume averaging theory. *Transp. Porous Media* 108 (2), 497–529. <https://doi.org/10.1007/s11242-015-0487-8>.